Battelle
The Business of Innovation

FINAL REPORT

EVALUATING THE POSSIBLE EXTENSION OF THE PROPANE CARGO TANK INSPECTION INTERVAL PHASE 2

NPGA/PERC Docket 12148

By
Rodney L. Osborne, Brian N. Leis, Ioan I. Feier,
and Thomas P. Forte

Energy Systems
Battelle Memorial Institute
505 King Avenue
Columbus, OH 43201

Prepared for
National Propane Gas Association
1899 L Street N.W.
Suite 350
Washington, D.C. 20036

September 2011

TABLE OF CONTENTS

List of Figures

List of Tables

EXECUTIVE SUMMARY

Currently, the U.S. Department of Transportation requires that propane cargo tanks ("bobtails") of MC330 and MC331 specifications be pressure-tested every five years [49CFR180.407] as part of the requalification process to continue in service. The pressure test is performed at 1.5 times the maximum allowable working pressure and is typically a hydrostatic test (commonly referred to as a "hydrotest"), with water as the test medium.

The required hydrostatic testing of bobtails is a burden to the propane industry for several reasons. Bobtails must be taken out of service for a period of up to a week. Water is introduced into the tank, which can be detrimental to the tank and to the fuel contained in the tank. Before being put back into use, the container must be completely free of any water. Practically speaking, the removal of bobtails from propane service can hamper a company's operations.

The National Propane Gas Association conducted a survey (NPGA 2001) to determine whether companies that perform the 5-year hydrostatic test requirement had experienced a significant number of failures. None of the 203 survey respondents reported a hydrotest failure for tanks of less than 3500 gallon capacity. Based on the results of this survey, the NPGA released a Request For Proposals to build the technical case for a change to the federal regulations. The ultimate goal of the project was to pursue a change to the federal regulations and the hydrostatic testing period for tanks on MC 330- or MC 331-specification cargo tank trucks exhibiting the following characteristics: non-quenched and tempered, 3,500 gallons or less and used in dedicated propane service.

Battelle has executed three phases of a project to consider the technical aspects of an extension to the current five-year hydrotest period. In Phase 0, Battelle performed a feasibility study to determine if the DOT was open to discussing a change to the inspection period. The study included a review of international standards that addressed cargo tank inspection periods. In Phase 1, Battelle developed crack growth models to estimate the time to failure of a tank that has undergone several pressure cycles. The pressure cycles were simplifications of daily and seasonal ambient temperature swings. When the crack growth model was exercised with the pressure cycles only, the estimated time to rupture was more than 2000 years.

In this Phase 2 work, an instrumented cargo tank on a truck chassis was subjected to actual road loads, and these loads were extrapolated for many years as the basis to determine the estimated life of the tank. The results of the crack growth modeling showed that the projected life of the tank was decades to centuries for initial crack sizes of less than 20% wall thickness. To then apply those results to other bobtail/tank combinations, the project team obtained photos of over 60 bobtail units currently in service. The team cataloged these units based on the type of tank-to-chassis mounting methods. One characteristic that was cataloged was the welding pattern of the longitudinal rail to the weld pad. This particular characteristic was modeled in a stress analysis code to determine the sensitivity of the weld pad configuration. The analysis indicated this variability of the weld pad could significantly increase the stress at the edge of the weld pad. The increase in stress at this tank high-stress point reduces the projected service life of the tank by an order of magnitude. This result was unexpected, and it precluded generalizing the results for the Trinity-Signature bobtail unit to other geometries.

Battelle also evaluated critical defect sizes as a function of steel properties and pressure and determined the consequences in terms of leak-before-rupture. This analysis considered the intent of the hydrotest, specifically the utility of the hydrotest to expose the presence of a significant crack in the vessel. Consistent with full-scale tests, it was found that with the toughness of modern vessel steels (Charpy energy > 25 ft-lbs), significant cracks of over 15 inches in length do not grow to failure during a hydrotest, or even result in a vessel leak. It was found that vessels made of steels with a relatively low Charpy energy of 5 ft-lb have a minimum crack size that also resisted the growth of deep cracks at typical hydrotest pressures, with cracks over 12 inches not causing a leak (and definitely not rupture). Thus, a vessel with a smaller crack size is not likely to fail (leak, much less rupture) during a hydrotest. A crack size of over 18 inches would be required for failure to occur during a hydrotest, but as mentioned earlier, the vessel will leak with a crack of this size, not rupture. It is also likely difficult to force a vessel to split with a crack of this size, in that a hydrotest pump may not be able to overcome the leak volume to grow the crack longer. Based on the ability of bobtail tanks to contain large deep cracks, and the observed leak-before-rupture behavior, the most conservative inspection method for these large cracks is a visual inspection. Moreover, because the hydrotest fails to expose large deep cracks it is ineffective and so inappropriate to inspect vessels in bobtail service, even those with relatively lower toughness. Visually inspecting these vessels on an annual basis is more conservative than the hydrotest. A vessel would likely be removed from service due to the presence of a visible crack, even though that crack may not leak and could therefore pass a hydrotest.

NPGA has sought to obtain research data that would support an industry recommendation to DOT to extend the requalification period from 5 years to 10 years. Battelle has concluded that the analysis and data generated as part of this study supports such a recommendation for tanks meeting the following requirements:

- In dedicated propane service
- Sized less than 3500 gallons water capacity
- Meeting DOT MC-331 specifications
- Constructed of one or more of the following materials:
    - Non-quenched and tempered (NQT) SA-612 steel
    - Non-quenched and tempered (NQT) SA-202 or SA-455 steels, provided the materials have full-size equivalent (FSE) Charpy-vee notch (CVN) energy test data that demonstrate 75% shear-area ductility at 32F with an average of three or more samples greater than 15 ft-lb FSE, with none less than 10 ft-lb FSE.

1. BACKGROUND

Currently, the U.S. Department of Transportation requires that propane cargo tanks ("bobtails") of MC330 and MC331 specifications be pressure-tested every five years [49CFR180.407] as part of the requalification process to continue in service. The pressure test is performed at 1.5 times the maximum allowable working pressure and is typically a hydrostatic test (commonly referred to as a "hydrotest"), with water as the test medium. To pass the test, the container must hold the pressure for 10 minutes without exhibiting leaks, distortion, or excessive permanent expansion.

The required hydrostatic testing of bobtails is a burden to the propane industry for several reasons. Bobtails must be taken out of service for a period of up to a week. Water is introduced into the tank, which can be detrimental to the tank and to the fuel contained in the tank. Before being put back into use, the tank must be completely free of any water. Practically speaking, the removal of bobtails from propane service can hamper a company's operations.

The National Propane Gas Association conducted a survey (NPGA 2001) to determine whether companies that perform the 5-year hydrostatic test requirement had experienced a significant number of failures. None of the 203 survey respondents reported a hydrotest failure for tanks of less than 3500 gallon capacity. Based on the results of this survey, the NPGA released a Request For Proposals to build the technical case for a change to the federal regulations. The ultimate goal of the project was to pursue a change to the federal regulations and the hydrostatic testing period for tanks on MC 330- or MC 331-specification cargo tank trucks exhibiting the following characteristics: non-quenched and tempered (NQT), 3,500 gallons or less and used in dedicated propane service.

In Phase 0 of this project [Battelle 2005], Battelle performed a feasibility study for the National Propane Gas Association (NPGA) to determine if the DOT was open to discussing a change to the inspection period. Staff from DOT's Research and Special Programs Administration (RSPA), now the Pipeline and Hazardous Materials Safety Administration (PHMSA) indicated that they were open to reviewing engineering analyses that could show an equivalent level of safety for an extended inspection period. The study also reviewed international standards that addressed cargo tank inspection periods. Many international standards are very similar to those of the United States, and some countries require no inspections (e.g., Mexico) or require no periodic inspections after the initial construction inspection (e.g., Australia). Based on the results of this phase of work, NPGA funded a Phase 1 effort. The Phase 1 report [Battelle 2007] detailed the results of fracture growth models to estimate the time to failure of a tank that has undergone several pressure cycles. The pressure cycles were simplifications of daily and seasonal ambient temperature swings. When the crack growth model was exercised with the pressure cycles only, the estimated time to rupture was more than 2000 years. In this Phase 2 work, an instrumented cargo tank on a truck chassis was subjected to actual road loads, and these loads were extrapolated for many years to determine the estimated life of the tank. While the lifetimes predicted using these methods for the tested truck were well beyond a hydrotest period (over 100 years for the tested loading cases), extending the analyses to other tank/mounting configurations beyond the tested truck proved difficult. The project team then considered a leak-before-rupture analysis. This analysis considered the intent of the hydrotest, specifically the utility of the hydrotest to expose the presence of a significant crack in the vessel. The sizes of

cracks were calculated, and the viability of alternative inspection techniques, including a visual inspection, was considered as an alternative to hydrotesting.

This Phase 2 report documents the work performed on the project.

2. INITIAL COMPUTATIONAL MODELING

Approach

As in Phase 1, a fracture mechanics approach was used to estimate the miles-to-failure using a crack growth analysis. The analysis assumed an infinitely sharp crack existed in the tank and the tank was subjected to normal over-the-road service loading. It is customary to assume the presence of an infinitely sharp crack to approximate the worst-case condition, as the sharp tip has the highest stress concentration factor. In Phase 1, the loads were due to seasonal and daily temperature changes of the saturated liquid propane. In Phase 2, the loads due to over-the-road driving with different amounts of propane lading were used. The cracks were positioned at the site of the maximum stress in the tank, and were assumed to be oriented perpendicular to the maximum principal stress – the worst case orientation. The size of the assumed crack was varied to assess the sensitivity of the service life. In both phases, upper bound crack growth rate data were used to compute the shortest, i.e., conservative, service lives, and the crack size at failure was based on the ductile flaw growth model [Leis, et al. 1991].

The over-the-road loading data used in the analysis were derived from strain measurements using strain gages. The strain gages were installed on the tank at locations determined using a finite element (FE) stress analysis model that was subjected to a set of specific load cases derived from ASME (ASME) and DOT [49CFR178] design code requirements. Details of the tank geometry, the stress analysis and the strain measurement program are described in the following sections of this report.

Tank Geometry and Finite Element Model

Figures 2 and 3 show the propane truck that was used to acquire the strain data used in the crack growth analysis. Some of the instrumentation cabling is visible on the sides of the tank in these photographs. The tank tested was designed and fabricated by Trinity Industries, Inc. (Dallas, TX). The tank was a 3200 gallon water capacity vessel, made of NQT steel and manufactured to the MC 331 specification. The tank was mounted to a 2005 International 4300 chassis by Signature Truck Systems (Clio, MI). Figure 1 shows the relevant data plates and certification stamps from the truck and tank.

The next several figures show details of the tank and the corresponding features of the finite element (FE) model. Figure 4 shows the FE model of the tank, along with the tank rails and the frame rails of the truck. Figure 5 shows the interior baffle and baffle-to-tank wall attachment brackets. Figure 6 shows the interior of the FE model and the baffle and its attachments. Figure 7 shows the underside of the tank and one of the six gussets (three per side) that attach the weld pad to the tank rails. Figure 8 shows a similar view of the FE model.

Figure 1. Data and certification information for International truck and Trinity cargo tank.

Figure 2. Propane truck used to acquire the over-the-road strain data – side view.

Figure 3. Propane truck used to acquire the over-the-road strain data – rear-quarter view.

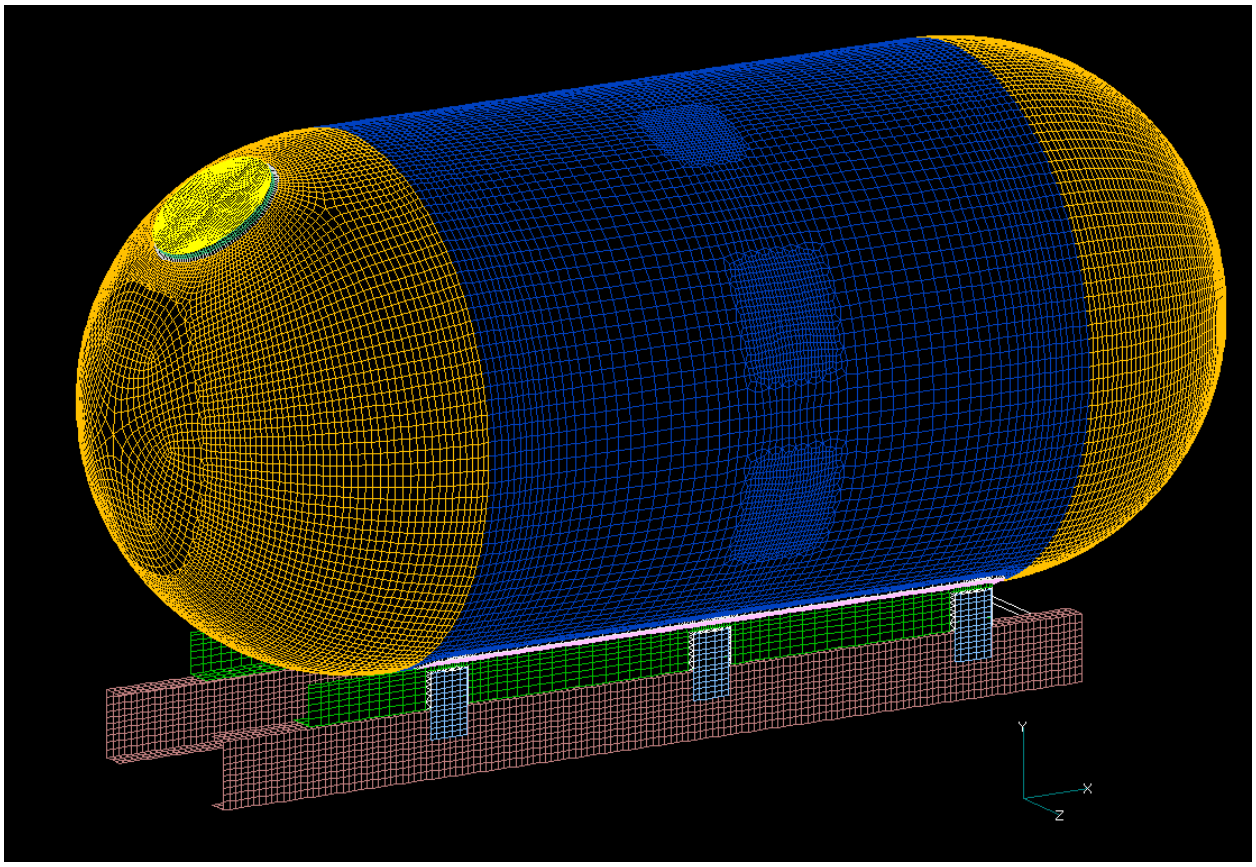

Figure 4. Finite element model of the tank, tank rails and truck frame rails – rear-quarter view.

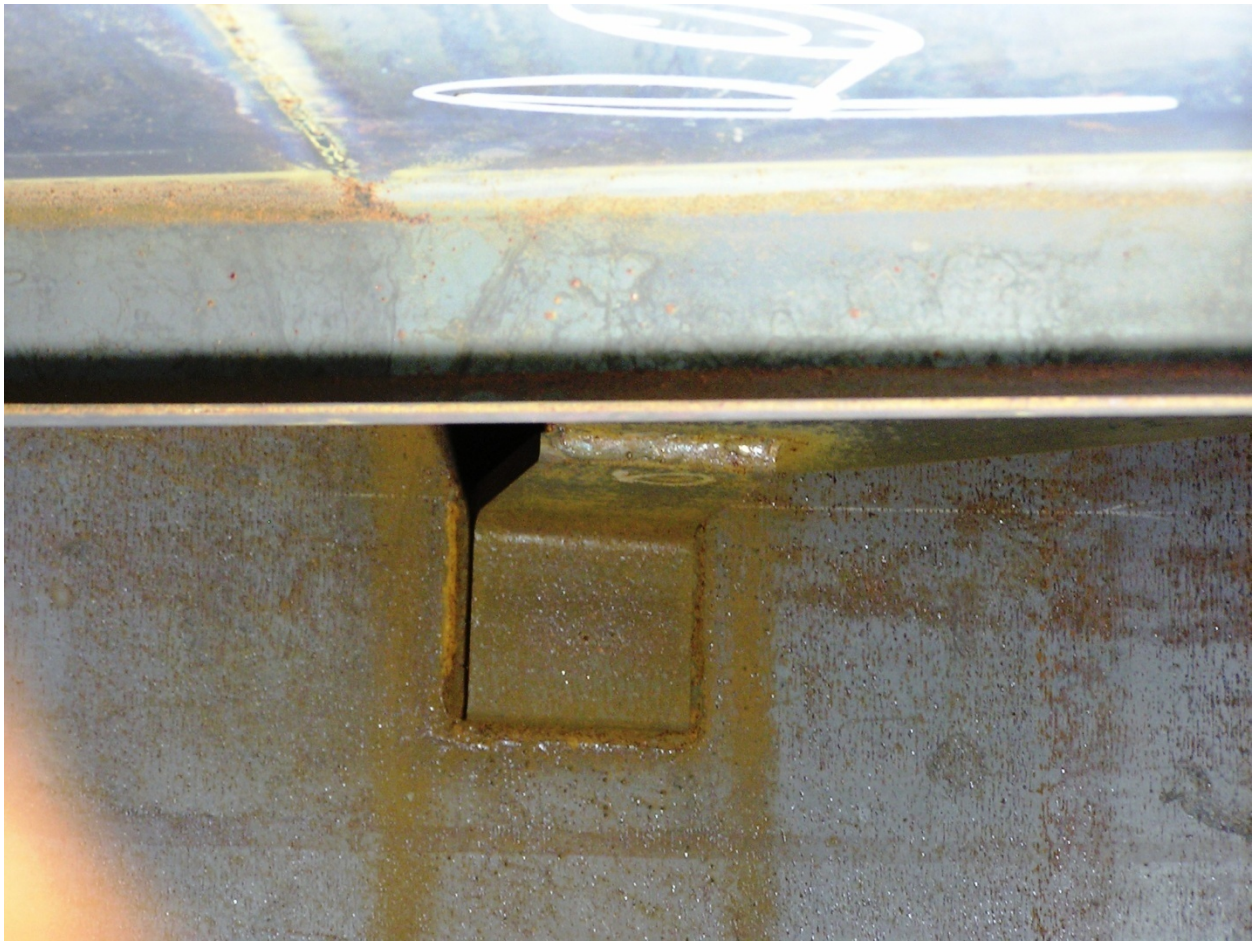

Figure 5. Tank internal baffle and baffle attachment to tank wall.

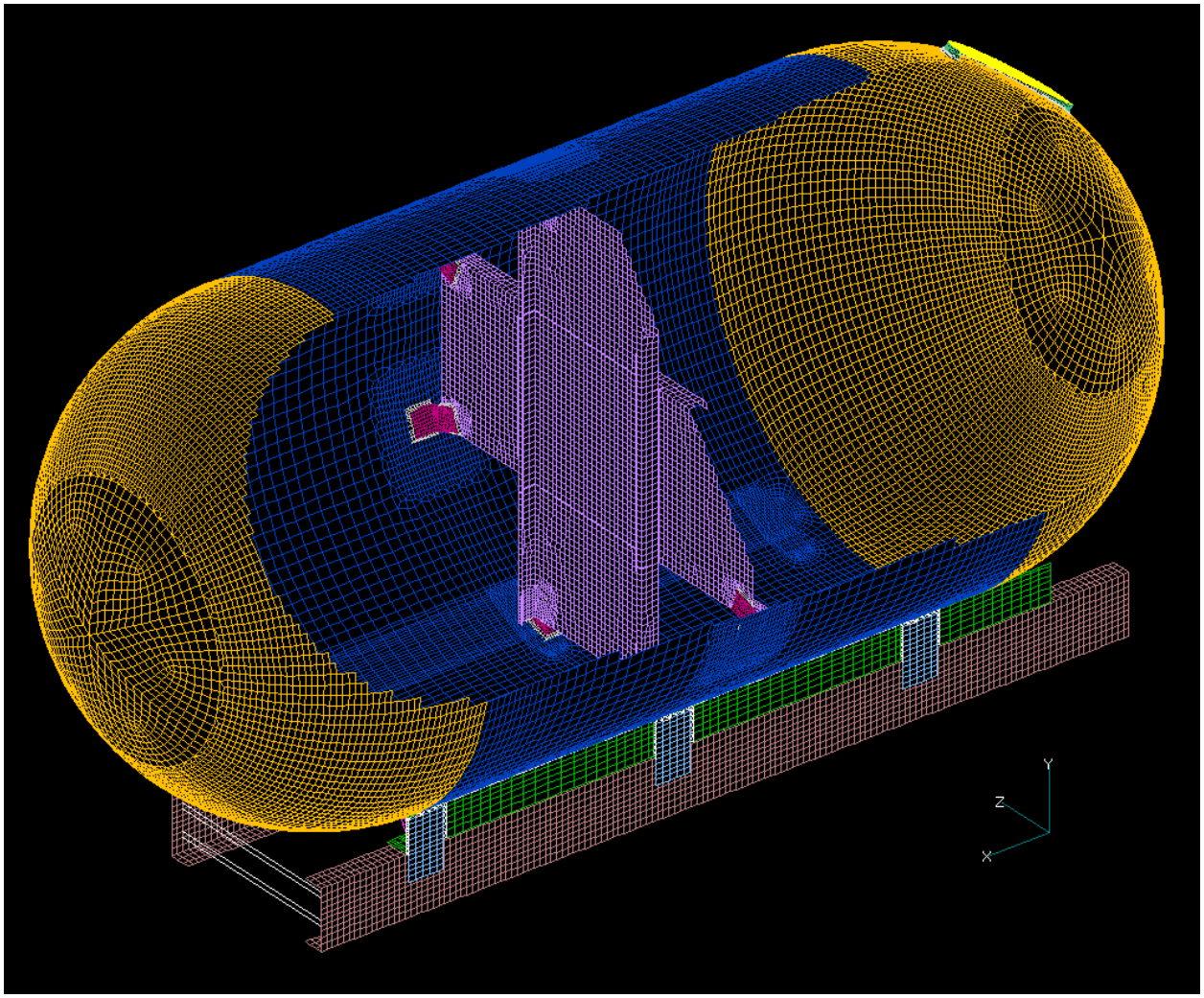

Figure 6. Finite element model of the tank showing interior baffle structure.

Figure 7. Underside of tank showing the weld pad and one of the six pad-to-tank rail gusset.

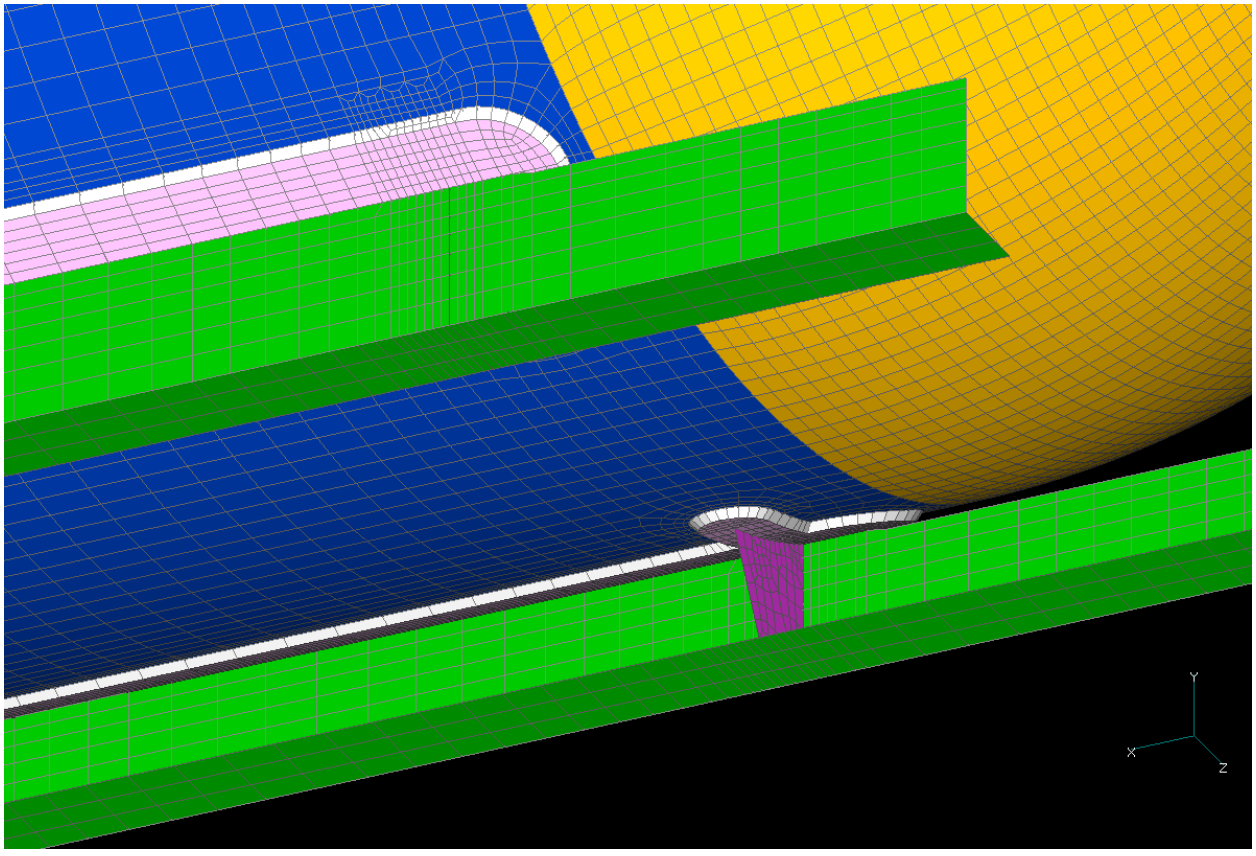

Figure 8. Finite element model of the tank showing pads that attach the tank to the tank rails, pad-to-tank welds and one of the six pad-to-tank rail gussets.

Stress Analysis

The primary purpose of the FE model was to identify high stress locations in the tank wall. The model included the pressure boundary of the tank, including the pressure boundary welds, as well as the internal baffle and the supporting structures and all relevant baffle and support welds. In addition, the model included the two longitudinal frame rails of the truck chassis, the attachment plates used to bolt the tank to the truck chassis, and the rear suspension attachment locations. The model was constructed of first order shell elements.

Boundary conditions included springs-to-ground that were attached to the suspension attachment points on the truck chassis. The forward end of the chassis frame rails were attached to one another through springs that represented the stiffness of the frame cross member and springs to ground.

All materials were steel having an elastic modulus of 29×10^6 psi and a Poisson's Ratio of 0.32. Because the model was elastic, the stresses and strains were proportional.

A total of twelve load cases were evaluated using the FE model. In these analyses, the acceleration due to gravity, g was 32.2 fps^2.

- Internal pressure, 250 psi
- Weight of the tank and support structure:
  - 1g Vertical
  - 1g Longitudinal
  - 1g Lateral
- Weight of the propane:
  - 1g Vertical hydrostatic fluid pressure
  - 1g Longitudinal hydrostatic fluid pressure
  - 1g Lateral hydrostatic fluid pressure
- Torsion (one rear wheel set unsupported)
- Combined load cases – the following included the weight of the tank and propane:
  - Pressure + 1.7g Vertical
  - Pressure + 0.7g Longitudinal
  - Pressure + 0.4g Lateral
  - Pressure + 1.7g Vertical + 0.35g Longitudinal+ 0.2g Lateral

The results of the stress analyses were used to construct a set of maximum stress sites for each load case. The strain gages used in the road testing were placed at these sites in order to capture the greatest response of the tank.

Because it was impractical to place strain gages on the inside of the tank, the FE results were used to infer the magnitude of the through-wall bending stresses that could be present in addition to the membrane strains in the tank wall. Figure 9 illustrates the situation where the stress on the inside wall is greater than that on the outside wall of the tank.

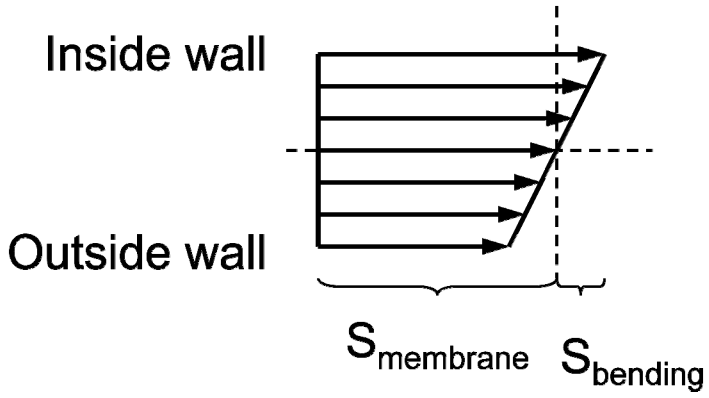

Figure 9. Schematic illustrating the stress component directions through the tank wall.

A list of the high-stress sites was created from the collection of FE results. The list included local Bending Factors, based on the following ratio:

$$\text{Bending Factor} = \frac{Stress_j^{inside}}{Stress_j^{outside}} \qquad Eqn\ 1$$

In some cases, the stresses were greater on the inside surface than on the outside surface, in which case the Bending Factor would be greater than 1. To be conservative, the Bending Factor used for the life assessment at each site was the greatest of all of the Bending Factors computed for that site, regardless of the loading case that produced it. This approach ensured that the greatest stress on the inside wall surface was used.

The following list summarizes the steps used to determine the Bending Factor values used in the life assessment analyses:

1. Identify and list model elements corresponding to each strain gage location. Note, some of the load cases were not symmetric right-to-left; therefore the elements on both sides of the vehicle were included in the list.
2. Recover stresses for each element in the list for each analysis case
3. For each stress component direction in each element, compute the Bending Factors for all analysis cases.
4. To be conservative, the Bending Factor that provided the greatest stress on the inside wall was selected for each strain gage site, regardless of actual stress direction or gage orientation

Pressure Stress. The maximum principle stresses on the outside surface (element top surfaces) of the tank wall corresponding to an internal pressure of 250 psi are shown on Figure 10. For this symmetric loading case, the maximum stresses were observed at the ends of the pads. This result was typical of the all of the load cases considered.

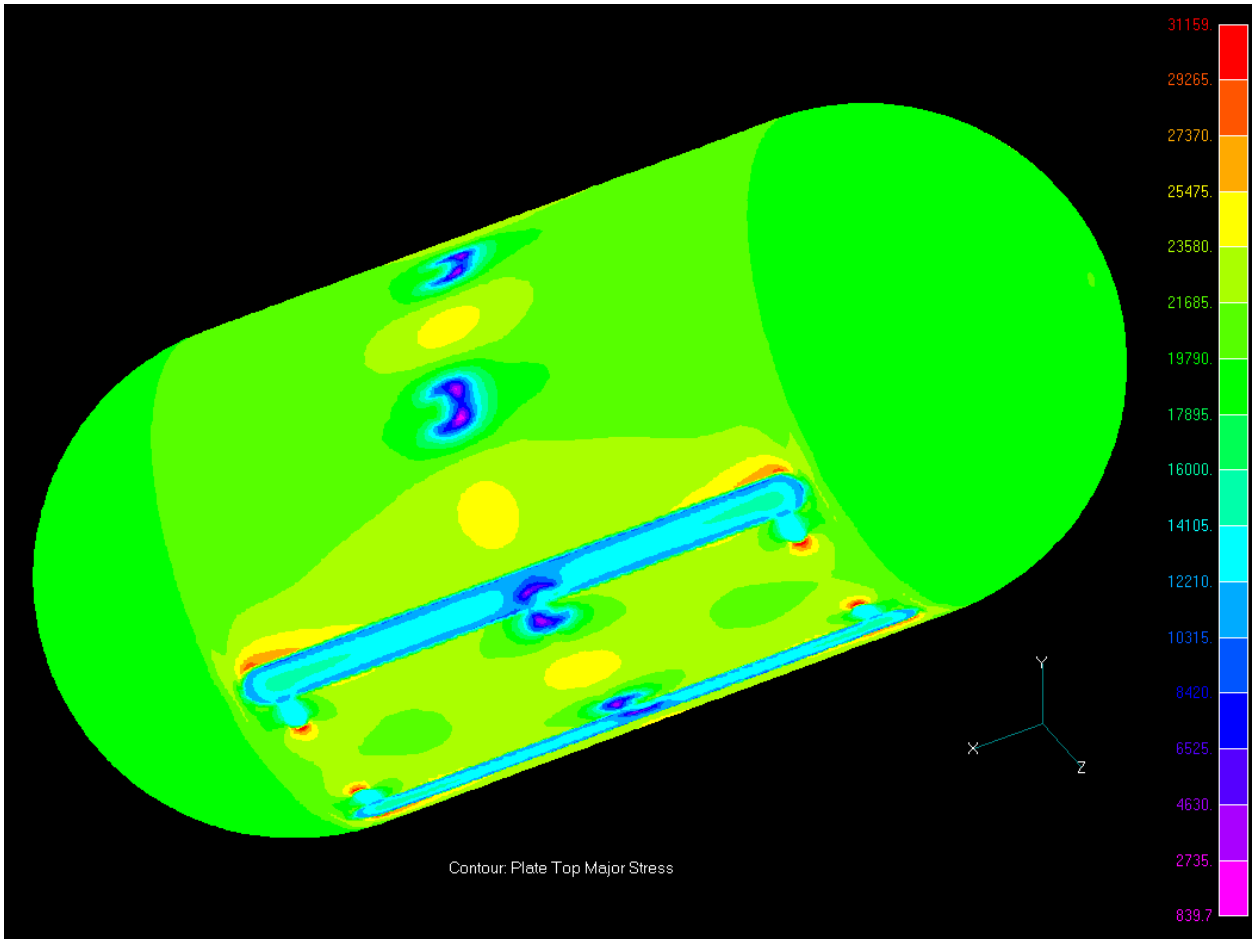

Figure 10. Maximum principle stresses on the outside surface (top) of the tank wall for 250 psi internal pressure.

Quasi-Static Dynamic Loading. The combined load cases defined above were used to account for a range of dynamic loading cases that the truck would experience on a random basis. These cases were selected based on experience with similar vehicles [ASME; Rogers 2006].

Location of Sensors and Transducers. At each highly stressed site identified with the FE model, two strain gages were mounted so that the stress at the weld toe could be determined by extrapolating the measured strains. Figure 11 shows the typical strain gage arrangement for the extrapolation. Each pair of strain gages used for extrapolation constituted a "strain transducer." Note, not all gages were used in pairs and no correction was made when one gage within a pair failed to provide useable data. Figure 12 shows a graphical and an actual strain gauge installation.

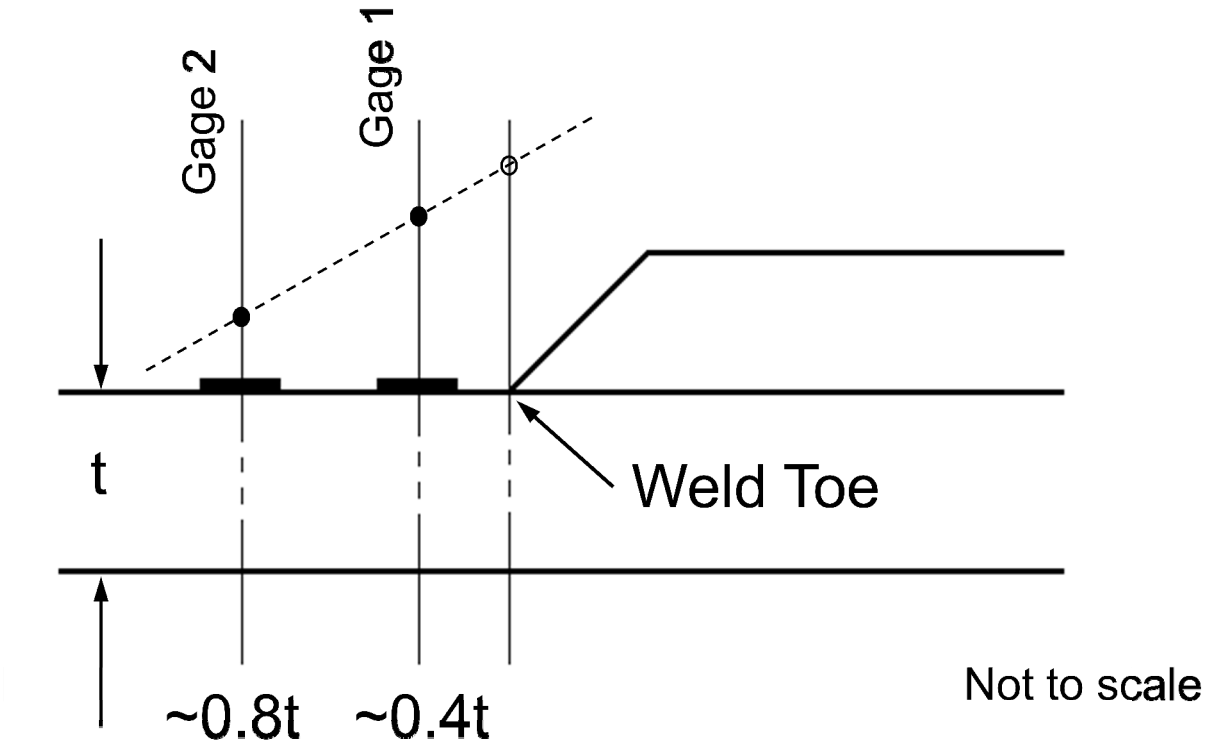

Figure 11. Typical strain gage arrangement for the extrapolating stresses at the weld toe.

Over-the-Road Stresses Applied to the Tank. The measured strains were used to compute stresses that were applied to the tank in the crack growth analysis, using Hooke's law. Stresses were computed for the outside tank wall surface where the strains were measured and on the inside using the greatest Bending Factor determined for the location where the strains were measured. The stresses were then reformulated to match the functional form used for the stress intensity factor, K_I shown in Figure 13 and Equations 2 and 3 [Anderson 2003].

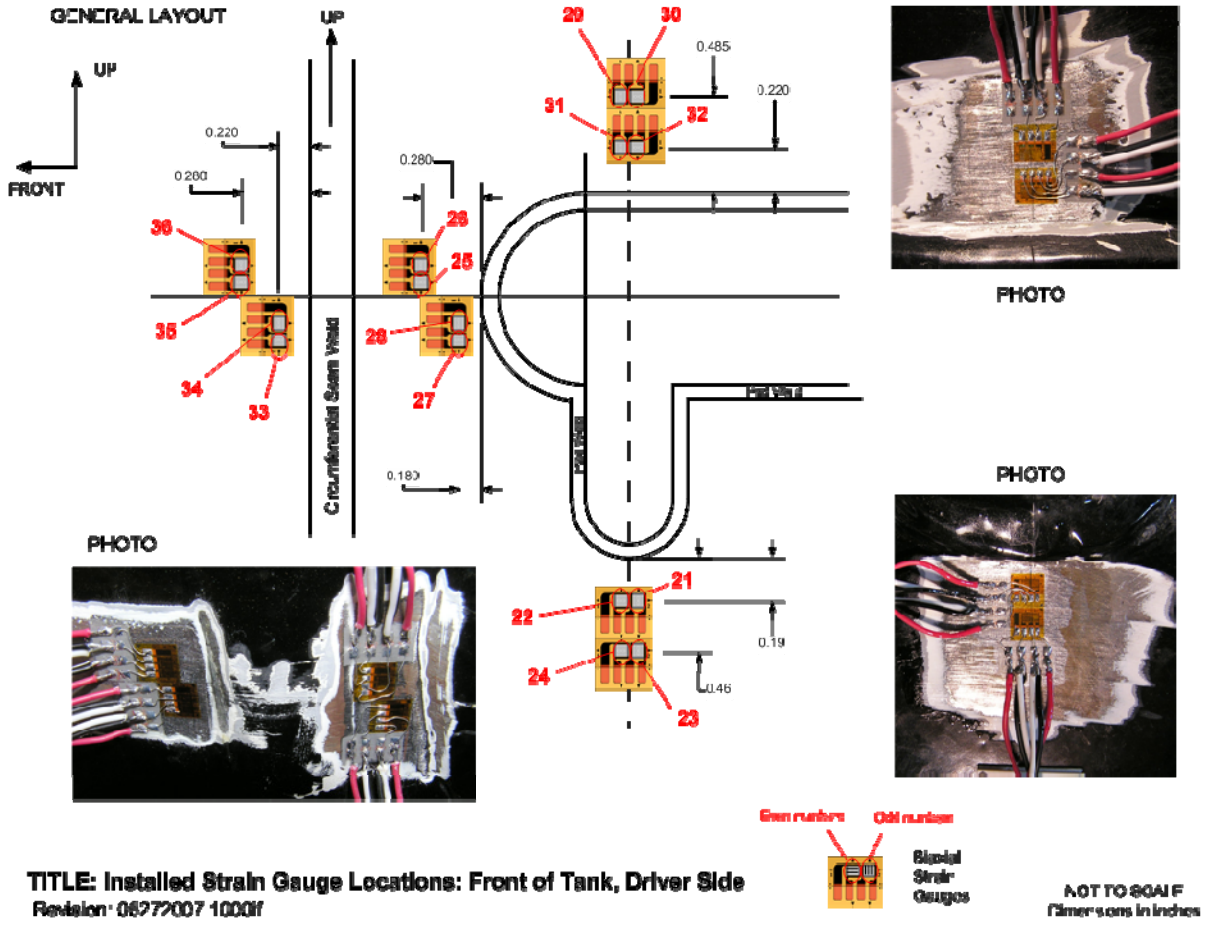

Figure 12. Graphical representation and actual installation of strain gauges.

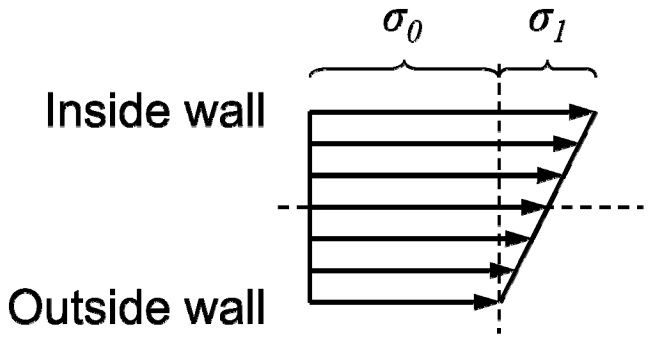

Figure 13. Stress component definitions used in the stress intensity factor, K_I.

$$K_I = \left[\sigma_0 G_0 + \sigma_1 G_1 \left(\frac{a}{t}\right) + \sigma_2 G_2 \left(\frac{a}{t}\right)^2 + \sigma_3 G_3 \left(\frac{a}{t}\right)^3 + \sigma_4 G_4 \left(\frac{a}{t}\right)^4 \right] \sqrt{\frac{\pi a}{Q}} \qquad \text{Eqn 2}$$

where
σ_i = stress coefficients
G_i = geometric coefficients
a = crack length
t = thickness
Q = elliptical integral

$$\sigma(x) = \sigma_0 + \sigma_1 \left(\frac{x}{t}\right) + \sigma_2 \left(\frac{x}{t}\right)^2 + \sigma_3 \left(\frac{x}{t}\right)^3 + \sigma_4 \left(\frac{x}{t}\right)^4 \qquad \text{Eqn 3}$$

where
$x = 0$, on exterior surface
$x = t$, on interior surface

Equations 4 and 5 provided the relationships required to apply the recoded stresses to the stress intensity factor, K_I in Equation 2.

$$Stress_{Outside} = Stress_{Recorded} = \sigma_o \qquad \text{Eqn 4}$$

$$Stress_{Inside} = Bending\ Factor \cdot Stress_{Recorded} \qquad \text{Eqn 5}$$
$$= \sigma_o + \sigma_1$$
where
$$\sigma_1 = (Bending\ Factor - 1) \cdot \sigma_o$$

$$note: \sigma_2 = 0, \sigma_3 = 0, \sigma_4 = 0$$

Crack Growth Analysis (Pressure Cycles plus Over-The-Road Stress Cycles)

The service life of the tank was estimated via a crack growth analysis. The crack growth analysis procedure consisted of selecting an initial crack size that could exist in the tank wall and then using the recorded stress (strain) data to analytically grow the crack until it was large enough to cause the tank to rupture. In each case considered, the crack penetrated the tank wall and caused a leak before the rupture was predicted. This is an important finding because it might be possible to detect the leak before a rupture might occur.

In Phase 1, the crack growth analysis was used to estimate the service life due to pressure cycles caused by daily and seasonal temperature changes of the saturated liquid propane in the tank. The lives predicted in Phase 1 for these pressure variations were long compared to the currently mandated retest interval. In this phase, the same crack growth analysis procedure was applied using the over-the-road stresses (strains) to assess the service life.

In each project phase, the crack growth analysis was conducted by numerically integrating the analytical equation used to represent the crack growth rate data for the tank steel. Details of the crack growth analysis were presented in the Phase 1 report [Battelle 2007].

3. TRUCK/TANK DYNAMIC TESTING

The test program was conducted in three stages: 1) small obstacle (bump) testing, 2) public road driving, and 3) test track driving.

In the bump testing, the truck was driven over relatively small bumps (similar to speed bumps, see Figure 14). During the bump loading, the loads and frequency responses on the tank were analyzed for various speeds and lading fill levels while the truck was driven between the fuel-loading depot and the bump-testing course. Once baseline bump tests were completed, the truck was driven over a representative public road course. This course was selected to bound the expected public road exposure of bobtails. This test plan is shown in Table 1. Five discrete days are shown in the table ("A" to "E"), however some of the test days were replicated, and there were times that the test sequence for a particular day was not completed and the test was either resumed or restarted on the next testing day.

Using the data from the bump testing, the FE structural model was exercised to refine the placement of the strain gauges. This data was used to select the road conditions that were used on the test track at the Transportation Research Center Inc. (http://www.trcpg.com/Durability_Testing.htm). The TRC is a multi-variable facility in the central Ohio area. The course has loading areas such as high slopes, cobblestones, high-crowned intersections, inline, and staggered potholes. Various vehicle speeds and lading fill levels were used for this testing also. Figure 15 shows some of the obstacles on TRC's Durability Course. The test plan for TRC's course is shown in Table 2. Again, similar to the bump testing, the discrete days listed in Table 2 ("AA" to "FF"), some of the test days were replicated, and there were times that the test sequence for a particular day was not completed and the test was either resumed or restarted on the next testing day.

Figure 14. Bump Testing.

Table 1. Test plan to characterize the truck/tank/propane dynamics.

Day*	Purpose	Locations	Tank Fill Level	Route Distance
A	Start	Columbus	Empty	--
	Over-the-road data	Columbus to WJ**	Empty	18 mi
	Define dynamic response of truck and tank	WJ driveway (single and multiple bump testing)	Empty	--
	End	WJ	Empty	--
B	Start	WJ	Empty	--
	Over-the-road data	WJ to Fuel Depot	Empty	31 mi
	Fill operation	Fuel Depot	Fill to 100%	
	Over-the-road data	Fuel Depot to WJ	Full	31 mi
	Define dynamic response of truck and tank	WJ driveway (single and multiple bump testing)	Full	--
	End	WJ	Full	--
C	Start	WJ	Full	--
	Over-the-road data	WJ to Fuel Depot	Full	31 mi
	Simulated delivery	Fuel Depot	Reduce to 66%	
	Over-the-road data	Fuel Depot to WJ	66%	31 mi
	Define dynamic response of truck and tank	WJ driveway (single and multiple bump testing)	66%	--
	End	WJ	66%	--
D	Start	WJ	66%	--
	Over-the-road data	WJ to Fuel Depot	66%	31 mi
	Simulated delivery	Fuel Depot	Reduce to 33%	
	Over-the-road data	Fuel Depot to WJ	33%	31 mi
	Define dynamic response of truck and tank	WJ driveway (single and multiple bump testing)	33%	--
	End	WJ	33%	--
E	Start	WJ	33%	--
	Over-the-road data	WJ to Fuel Depot	33%	31 mi
	Simulated delivery	Fuel Depot	Empty	
	Over-the-road data	Fuel Depot to WJ	Empty	31 mi
	End	WJ	Empty	--

* Day – nominally days were planned to be sequential, but periodically tests were repeated due to an incomplete test day (such as for data acquisition system issues or adverse weather).

** WJ – Battelle's research facility near West Jefferson, OH

Figure 15. TRC Durability Course Loadings, clockwise from top left: Frame Twist Humps, Cobblestones, Random Chuckholes, Washboard, Deep Chuckholes.

Table 2. Test plan to gather data for discrete events and for over-the-road operations.

Day*	Purpose	Locations	Tank Level	Route
AA	Start	WJ**	Empty	--
	Over-the-road data	WJ to TRC***	Empty	43 mi
	Safety inspection	TRC garage	Empty	--
	Discrete events	Skid pad	Empty	--
	Gather data on accelerated test course	Bus/Truck Durability and Cobblestone courses	Empty	--
	Off-road operation	Off-road course	Empty	--
	Over-the-road data	TRC to WJ	Empty	43 mi
	End	WJ	Empty	--
BB	Start	WJ	Empty	--
	Over-the-road data	WJ to TRC	Empty	43 mi
	Safety inspection	TRC garage	Empty	--
	Discrete events	Skid pad	Empty	--
	Gather data on accelerated test course	Bus/Truck Durability and Cobblestone courses	Empty	--
	Off-road operation	Off-road course	Empty	--
	Over-the-road data	TRC to Fuel Depot	Empty	63 mi
	Fill operation	Fuel Depot	Fill to 100%	
	Over-the-road data	Fuel Depot to WJ	Full	31 mi
	End	WJ	Full	--
CC	Start	WJ	Full	--
	Over-the-road data	WJ to TRC	Full	43 mi
	Safety inspection	TRC garage	Full	--
	Discrete events	Skid pad	Full	--

Day*	Purpose	Locations	Tank Level	Route
	Gather data on accelerated test course	Bus/Truck Durability and Cobblestone courses	Full	--
	Over-the-road data	TRC to WJ	Full	43 mi
	End	WJ	Full	--
DD	Start	WJ	Full	--
	Over-the-road data	WJ to TRC	Full	43 mi
	Safety inspection	TRC garage	Full	--
	Discrete events	Skid pad	Full	--
	Gather data on accelerated test course	Bus/Truck Durability and Cobblestone courses	Full	--
	Over-the-road data	TRC to Fuel Depot	Full	63 mi
	Simulated delivery	Fuel Depot	Reduce to X%	
	Over-the-road data	Fuel Depot to WJ	X%	31 mi
	End	WJ	X%	--
EE	Start	WJ	X%	--
	Over-the-road data	WJ to TRC	X%	43 mi
	Safety inspection	TRC garage	X%	--
	Discrete events	Skid pad	X%	--
	Gather data on accelerated test course	Bus/Truck Durability and Cobblestone courses	X%	--
	Over-the-road data	TRC to WJ	X%	43 mi
	End	WJ	X%	--
FF	Start	WJ	X%	--
	Over-the-road data	WJ to TRC	X%	43 mi
	Safety inspection	TRC garage	X%	--
	Discrete events	Skid pad	X%	--
	Gather data on accelerated test course	Bus/Truck Durability and Cobblestone courses	X%	--
	Over-the-road data	TRC to Fuel Depot	X%	63 mi
	Simulated delivery	Fuel Depot	Empty	
	Over-the-road data	Fuel Depot to WJ	Empty	31 mi
	End	WJ	Empty	--

* Day – nominally days were planned to be sequential, but periodically tests were repeated due to an incomplete test day (such as for data acquisition system issues or adverse weather).
** WJ – Battelle's research facility near West Jefferson, OH
*** TRC – Transportation Research Center, East Liberty, OH

Notes:

1. Truck was instrumented at Battelle, Columbus and was stored overnight at Battelle, West Jefferson. The truck was returned to Columbus after all tests were completed.
2. Single and multiple bump tests to characterize the vehicle dynamics were conducted on a WJ driveway. The driveway was closed for approximately 5 minutes per test run. Metal bumps were placed on the driveway for these tests.
3. The Fuel Depot was located in Canal Winchester, Ohio.
4. TRC mandates a daily safety inspection before the truck was permitted to use their test facilities. The inspection required approximately 2 hours to complete.
5. TRC's Off-Road course is located approximately 3 miles west of the main entrance to their facility.
6. Four propane levels were used to characterize truck/tank/propane the dynamics. Three propane levels were evaluated at TRC, namely full, empty and a third partially full level (40%), determined from the characterization testing results.
7. The accelerometers were moved as required during the dynamic characterization testing to better capture the truck/tank/propane dynamic response.

Once the data were collected during the test period, the data were processed and annotated with the test conditions, using MATLAB [MATLAB]. Figure 16 is a representative example of one data file. The top curve in the chart shows data from Strain Gauge #41 (located at the toe of the weld pad, driver's side, toward the front of the tank, see Appendix A), for a period of approximately 4000 seconds. The bottom curve shows the steering angle string potentiometer, indicating left and right turns. The data are annotated from using the notes from each data set (example shown in Table 3). Figure 17 is a map of the example test run.

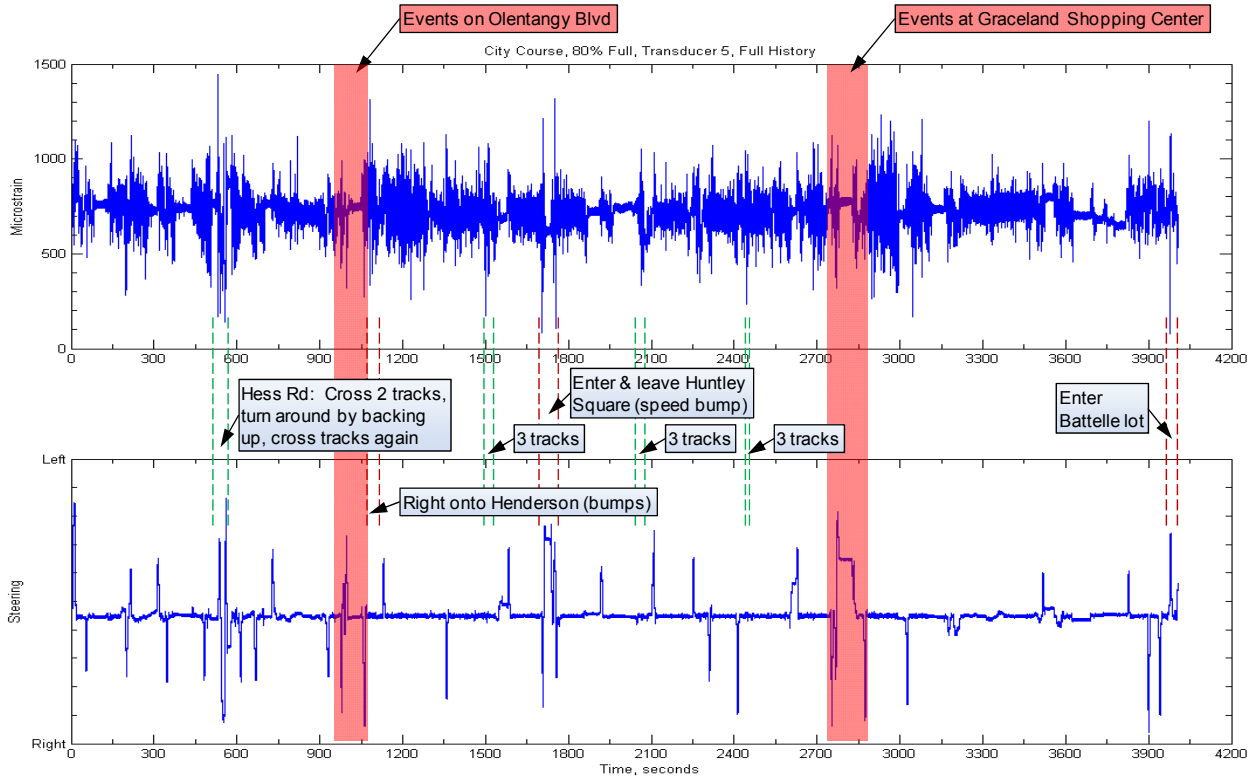

Events in red boxes were executed on "80% full" run only

Figure 16. Example processed data file, for Strain Gauge #41, collected on the City Road Course.

Table 3. Example of test run log, indicating events (turns, obstructions) encountered during the test.

1. Left (W) on 5th out of Battelle
2. Right (N) on Olentangy Rv.
3. Right (E), follow Olentangy Rv.
4. Left on John Herrick
5. Left on Woody Hayes
6. Right on Kenny Rd
7. Stop at traffic light, cross Lane
8. Right on Hess Rd
9. Railroad tracks 2x
10. Turn around by backing up
11. Railroad tracks 2x
12. Right on Kenny Rd
13. Right on Ackerman
14. Left on SR 315 (N)
15. Maintain 55 mph
16. Exit at Henderson
17. Right at exit (E) on Henderson
18. Right on Olentangy Blvd.
19. Turn around by backing
20. Right on Henderson (E), bumps
21. Left on N High St. (N), bumps on right side of lane
22. Right on Lincoln
23. Stop at Foster (stop sign)
24. Railroad tracks, 1x and 2x
25. Left on Sinclair
26. Cross SR 161
27. Right into Huntley Square parking lot
28. Speed bump exiting lot
29. Right (N) on Huntley
30. Left on Schrock
31. Railroad tracks, 2x, 1x
32. Left on Proprietors Rd.
33. Left on SR 161
34. Right on Sinclair
35. Right on Lincoln
36. Railroad tracks, 2x, 1x, then steel plate on road
37. Stop at Foster (stop sign)
38. Left on High
39. Right into parking lot for Graceland Shopping Center
40. Right on N High, bumps
41. Right on Henderson, bumps
42. Right loop to SR 315 (S)
43. Exit on Olentangy River Road
44. Left on King
45. Right on Battelle
46. Right on W 5th
47. Left into Battelle lot

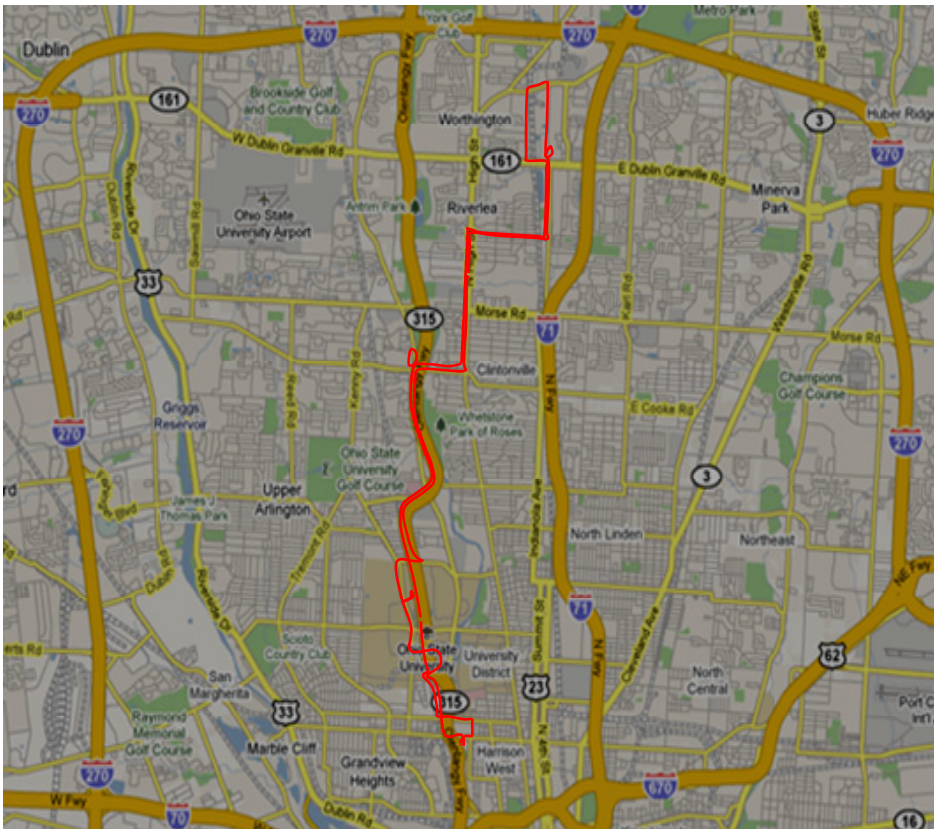

Figure 17. Example of a road course test run.

4. TANK LIFE ANALYSIS

Initial Crack Size Analysis

The initial crack size refers to the depth and length of an external, semicircular surface crack that was assumed to exist in the tank wall at the start of the simulated service that was analyzed in the life assessment. The initial crack sizes ranged from 10% to 70% of the wall thickness. As expected, the life increased with decreasing initial crack sizes.

Crack Orientation. The principle loading directions of the tank favor longitudinal (axial) and hoop (circumferential) crack orientations. Therefore, it was essential to consider both crack orientations in the life assessment. The effect of crack orientation was evaluated in detail for the strains measured at Transducer 5. For this location, the circumferential crack had shorter lives for all initial crack sizes, both with and without the Bending Factor. In addition, consider the following critical crack sizes* (total length) at failure for each orientation [Kastner 1981]:

- Circumferential crack:
  - With Bending Factor: ~3.3 inches
  - Without Bending Factor: ~10.8 inches
- Axial crack:
  - With Bending Factor: ~11.9 inches
  - Without Bending Factor: ~23.9 inches

These results were obtained when the load was applied to the circumferential crack as an equivalent pressure and as a constant through-wall stress. It was also observed that when the cracks where physically short, the growth was insensitive to the curvature of the tank wall.

Generation of Mixed Road-Data Set

Propane delivery operations include a mix of the test conditions. The data showed that the 80%-Full, City Course bounded the measured strain response, and that of all of the strain transducer sites, Transducer 5 experienced the greatest strains when the Bending Factor was applied. Without the Bending Factor, Transducers 5, 10, and 12 bound the response. To be conservative, only the City Course data, with the Bending Factor, were used in the life assessment.

A uniform mix of lading conditions, 0%-Full, 40%-Full and 80%-Full for the City Course was used in the life assessment. For analysis purposes, mixed usage refers to simulated operation derived by appending the data files from different routes and/or load levels into a single file in a predefined sequence for subsequent use in the life assessment. Table 4 shows a series of usage mixes for a representative propane delivery truck that was used to assess the sensitivity of the service life to various editing techniques for Transducer 5. Originally, editing was used to ensure that each of the three lading conditions was recorded on exactly the same route, because

* The failure criteria for the circumferential crack was based on Kastner's analysis which uses flow stress to assess failure, whereas the axial crack was based on the PAFFC analysis which uses flow stress and ductile tearing to assess failure.

the 80%-Full run included some events that were not included in the other two lading runs. Additional editing was done on the 80%-Full run to assess other variations in the route profile and the strain magnitudes. These edits are listed below.

1. 80 % full, AS-RECORDED – As-recorded data from the "80% full" route
2. 80 % full, CLIPPED – Removed largest eight strain excursions of the "80% full" file
3. 80 % full, FIXED – Removed events on Olentangy Blvd and at Graceland Shopping Center from the "80% full" data because they were not included in the "40% full" or "0% full" simulated operation runs
4. 80 % full, EDITED – Removed the RR crossings on Hess Rd from the "80 % full, FIXED" data
5. 80 % full, EDITED2 – Removed the maneuvers at Huntley Square Shopping Center from the "80 % full, EDITED" data

Table 4. Operational usage mixes used in the life assessment.

		Usage mixes				
		1	**2**	**3**	**4**	**5**
Repeating Sequence	1	80 % full	80 % full	80 % full, FIXED	80 % full, FIXED	80 % full, FIXED
	2	40 % full	40 % full	40 % full	40 % full	40 % full
	3	0 % full	0 % full	0 % full	0 % full	0 % full
	4	--	80 % full, CLIPPED	--	80 % full, EDITED	80 % full, EDITED2
	5	--	40 % full	--	40 % full	40 % full
	6	--	0 % full	--	0 % full	0 % full
	7	--	80 % full, CLIPPED	--	80 % full, EDITED	80 % full, EDITED2
	8	--	40 % full	--	40 % full	40 % full
	9	--	0 % full	--	0 % full	0 % full

Calculation of Estimated Tank Lives

The service lives predicted for each of the five usage mixes are shown in Figure 18. The variation in life for these mixes is minimal relative to the variation in life with initial crack size. Therefore, to better illustrate the variation in lives, Figure 19 shows a bar graph of only the predictions for an initial crack size of 10% of the wall thickness. The results in Figure 18

indicate that initial crack sizes smaller than approximately 25% of the wall thickness would have service lives greater than 10 years regardless of the usage mix considered in this investigation.

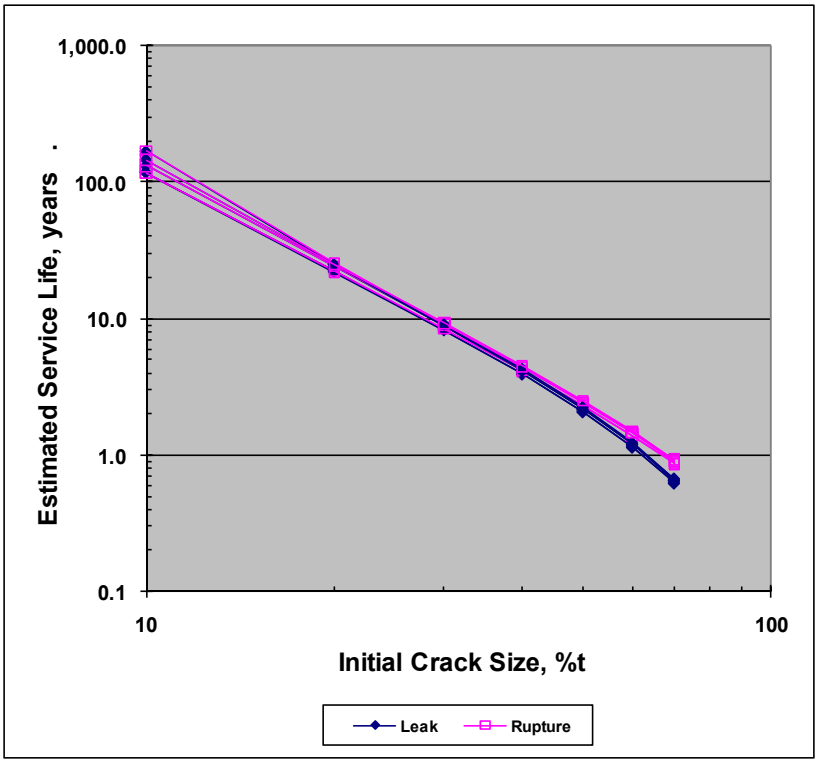

Figure 18. Predicted service lives for five usage mixes and a range of initial crack sizes.

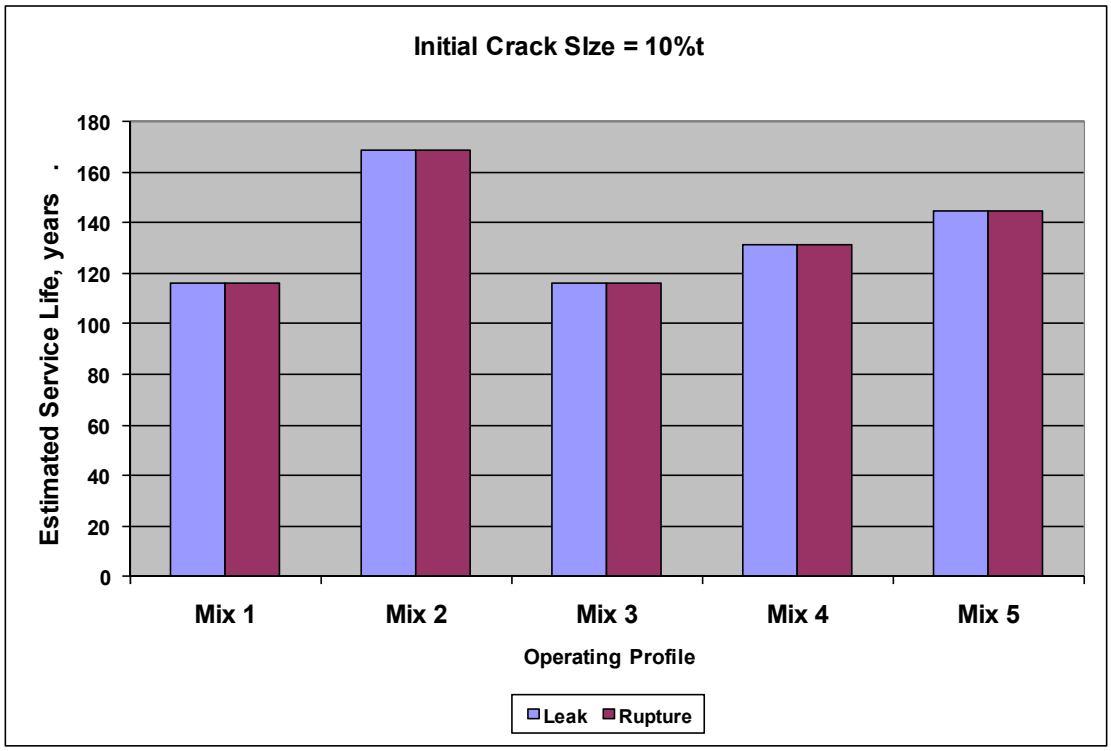

Figure 19. Predicted service lives for five usage mixes and an initial crack size of 10% of the wall thickness.

5. COMPARISON OF TESTED TANK AND OTHER TANKS IN POPULATION

In planning and conducting the research required for this effort, several different tank attachment designs were observed. The tank provided for the strain measurements was considered to be typical of a new construction. Important factors that could affect the predicted service life are the locations of the relative maximum stresses and the measured local inside and outside strains at these sites. Geometric features that could affect the stress conditions include: tank size, pad size and shape (e.g., continuous or intermittent pads; pad corner shape: round, square or angled, ratio of pad thickness to tank wall thicknesses), and the pad-to-frame rail attachments. In addition, other important features of the tank design and the truck include the slosh control baffle and the vehicles suspension.

Appendix C contains a collection of photographs of various tank-mounting configurations. Considering only the external, visible features of the tank mounting and ignoring the unseen internal baffles and the suspension system, three criteria were selected to assess the applicability of the results presented in this report to other tank configurations, namely:

- Pad length: continuous or intermittent
- Pad end geometry: round, square or angled
- Distance from the pad to tank weld to end of the pad support

The life prediction results were judged to be applicable to tanks that satisfy the following conditions: continuous pads with round or angled corner ends, and where the distance from the pad to tank weld to end of the pad support was equal to or greater than the tank instrumented for this program. Of the 75 tank/truck units observed, only 9 were believed to be of sufficient similarity that the analyses discussed above were directly applicable. The remainder of the units fell into one of two categories: 1) there was sufficient variation from the tested truck that extrapolations of the current results were not possible; or 2) there was insufficient certainty in the stress behavior due variation in the geometry. These results are discussed further in the next section.

6. ANALYSIS OF DEFECT RESPONSE TO PRESSURE AND LEAK BEFORE RUPTURE FOR BOBTAIL PROPANE TANKS

As part of the Phase 0 effort of this project, Battelle assessed whether the DOT might be open to discuss a change to extend this inspection interval. To gain a broader understanding, Battelle reviewed international standards that addressed cargo tank inspection periods. This review focused on tank integrity management practices and gathered for 15 countries. It was found that such practices typically used pressure testing with water to pressurize the vessel (a hydrostatic test ("hydrotest") at pressures up to 1.5 times the maximum allowable working pressure (MAWP). Further, it was found that these practices often involved re-hydrotesting at an interval that ranged for five to twenty years for regulators that required retests. But, it was also determined that the regulatory authorities in some countries did not requiring retesting, and that the US requirements were among the most stringent [Osborne 2005]. This favorable outcome coupled with a wait-and-see position from the regulator in a meeting between the PHMSA and Battelle[†] led to a second phase of this work, denoted Phase 1.

In Phase 1 Battelle developed a fracture-mechanics based model of defect growth from assumed defects at welds due to fatigue, to estimate the time to failure of a tank that has undergone in-service pressure cycles, as well as that due to the periodic hydrotesting. This pressure-cycles-only analysis made use of simple idealizations of daily and seasonal ambient temperature swings. When the crack growth model was exercised subject to pressure cycling, the estimated time to rupture was more than 2000 years. This very long period motivated Phase 2, which included a more accurate representation of both the loadings and the stresses they induce, with the loadings now considering all components that must be addressed in tank design.

Of all the loadings and the induced stresses that must be addressed in propane cargo tank design [e.g. 49CFR178.337.3], the loads due to over-the-road delivery are relatively uncharacterized without reference to a particular tank/truck design. Forces from the road transmitted through the truck chassis into the tank as functions of time and tank lading can be estimated but somewhat subjectively. As discussed previously, the current project included extensive over-the-road testing using an instrumented cargo tank on a truck chassis. For various reasons, this work focused on the Trinity-Signature bobtail tank/chassis and supporting truck-frame and tank

[†] For details on the attendees for the PHMSA and Battelle see Reference 2.

attachment. As discussed, strain gauges were used to quantify local strains, which were used in parallel with detailed stress analysis to infer local stress-strain response. The actual road loads were then extrapolated to represent many years of service, and used as input to determine the estimated life of the tank. As shown in Section 4 of this report, the results of the crack growth modeling showed that the projected life of the tank was from decades to centuries for initial crack depths less than 20% of the wall thickness.

With a view to generalize the outcomes for the specific bobtail design tested to the general population of bobtail designs in service, the project team obtained photos of over fifty bobtail units currently in use. These images were cataloged based on the type tank-to-chassis mounting methods, and other parameters. One important site cataloged was the geometry local to the longitudinal rail and the weldpad on the tank, as this vicinity was among those with the highest local stresses, and this parameter was considered a controlling factor for the magnitude of those stresses. This site was modeled in a numerical sensitivity study of the weldpad-rail geometry on local stress, which indicated variations in weldpad design could significantly increase the local stresses. The models used for this analysis are shown in Figure 20. Such results showed that the increase in stress for some configurations could cause an order of magnitude reduction in the projected service life of the tank. This strong sensitivity was unexpected, and precluded generalizing the results for extrapolating the analysis completed on the Trinity-Signature bobtail unit to other tank to truck rail geometries. This limited generality of life prediction to multiple geometries and configurations thus motivated consideration of alternative approaches to assess the need for and related interval for hydrotesting, as considered next.

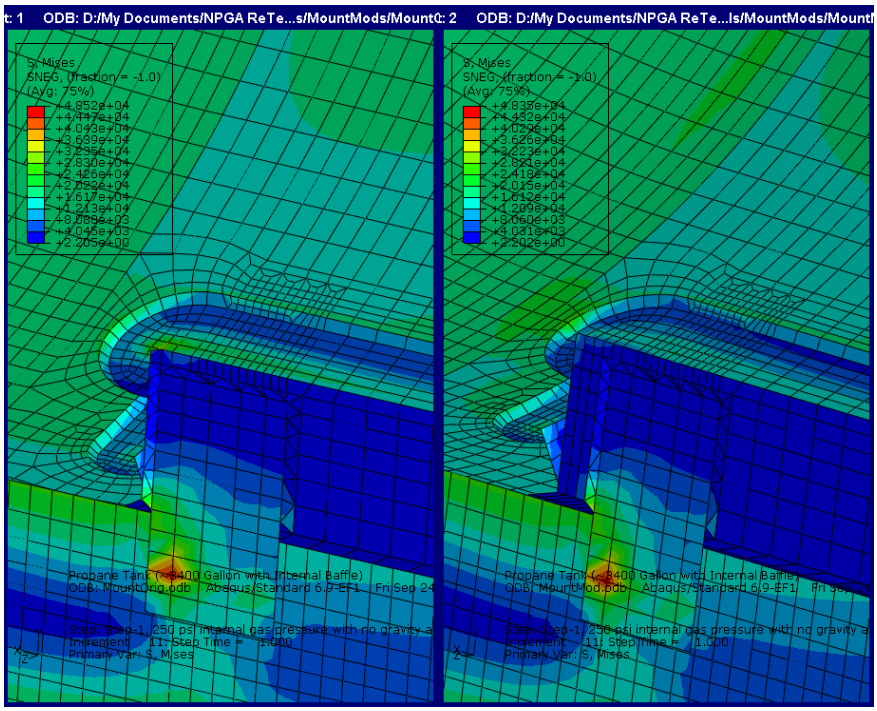

Figure 20. Finite Element analysis of varying distance from end of frame rail to end of weldpad.

Battelle has extensive experience with hydrotesting involving comparable steels [e.g. Leis 1991, Leis 2001]. This work has led to an understanding of when hydrotesting is beneficial, versus practically ineffective, and for such scenarios led to practical and technically sound inspection-based alternative integrity verification (AIV) schemes for gas-transmission pipelines[e.g. Leis 2000] that now are in field demonstration [e.g. Zhou 2008]. Accordingly, this technology has been used as the vehicle to consider the utility of hydrotesting for the bobtail application, and as appropriate develop and explore a practical alternative to the overly restrictive approach detailed above based on life cycle analysis. This section introduces the technology, and presents a simple, practical, and technically better alternative to the initial plan, while Appendix B presents the underlying concepts. The following sections present the outcomes prior to discussing the technology details on the premise that if the concept has practical merit there will be a motive to read about it and more broadly consider its utility for the present application.

Battelle briefly explored the implications of technology to quantify defect growth and critical defect sizes [Leis 2001] as a function of the steel properties and tank geometries of use in the Bobtail-tank industry. This led to contours of failure pressure as a function of defect depth and length, and determined the consequences of failure in terms of a leak-before-rupture analysis. If such analysis determines that very long and deep defects remain stable, and at worst leak if they breach the wall, then something as simple as visual inspection obvious as a large rust stain on the tank running from a gaping but very stable crack is viable. More critically, the work that led to the AIV approach noted above grew from the realization that hydrotesting was no longer a viable pressure proof-test [Leis 2000, Leis 2001: Appendix 7] – although it remained useful as a leak test.

Appendix B details the development of the plots that follow, and the underlying technology, while Reference 8 details its full-scale validation. Interested readers should consider those resources for related details.

Basis for Predicted Failure Boundaries

This analysis considered the intent of the hydrotest – specifically the utility of the hydrotest to expose the presence of a significant crack in the Bobtail vessel, which typically has been considered to require rupture during the hydrotest. Because the size of defects that grow in response to pressure is a function of the tank geometry and the steel's flow and fracture response, values typical of these parameters have been adopted consistent with industry history, standards, and tank designs. Given the range of tank sizes and wall thicknesses, and the range of steel grades and differences in their production over time, the Charpy vee-notch (CVN) energy (i.e., the toughness) has the greatest influence on the predicted outcome.

Steel grades used in propane cargo tanks have ranged historically from the alloy-steel SA-202 [SA-202], and other grades, with a shift to SA-612[SA-612] occurring from the early to mid 1980s [Auxier 2011]. The reason for this shift from a more highly alloyed steel to SA-612 was driven exclusively by supply and demand of certain elements, which led to significant cost increases [Auxier 2011]. SA-612 was widely available commercially for the wall thickness used in bobtail tanks as this transition occurred, with some industry opinion indicating that this grade reflects most of the bobtail production – but as is often the case exceptions are evident

[Mississippi Tank Co. 1987, Mississippi Tank Co. 2001]. Referenced to SA-202-Grade A and SA-612 (taken for plate thickness >0.5-inch), the specified minimum yield stress (SMYS) has ranged from a historic value‡ at 45 ksi (for SA-202) up to its current level at 50 ksi, while the specified minimum tensile stress (SMTS) has ranged from a historic value at 75 ksi for up to its current level 81 ksi. Accepting industry opinion, these values are adopted as typical of the tank production prior to as well as since the early 1980s.

Accepting that the shell geometry of the Trinity-Signature bobtail unit is representative of such tanks, and given that small differences in diameter and thickness do not significantly affect changes in the defect growth response to pressure in such tanks, the dimensions of that shell can be adopted as a basis to quantify this defect response. Because the toughness of the steel that comprises bobtail tanks has a first-order effect on the growth and stability of defects in such tanks, and even though some data show steels like SA-612 can have quite high toughness [Mississippi Tank Co. 2009], the fact remains that even today the CVN energy for Bobtail tank applications is not well quantified. Accordingly, the results that follow have been evaluated parametrically from a low CVN full-size equivalent (FSE) energy of 5 ft-lb up through 150 ft-lb.

The range of toughness selected follows in light of Battelle's archival data for pipe and vessel steels, data for which are shown in Figure 21. These data reflect the upper-shelf (fully-ductile) energy, also called the plateau energy such that the y-axis in this figure is labeled CVP for Charpy-vee plateau energy, while the x-axis indicates the year of production over the interval from the late 1920s up through 2000. Significant scatter is evident in this figure, as is a clear trend to higher toughness levels emerging about the 1970s. It is apparent that earlier vintage steels had higher toughness than did many steels into the late 1960s, after which the just noted increasing trend develops. It is widely known that the properties desired in construction steels – strength, ductility, toughness, and weldability (for some also corrosion resistance) are inter-related through their chemistry and processing, and the resulting microstructure. It is also broadly understood that the sulfur content of the steel and its processing for sulfide shape control significantly influence CVN energy, which is considered later as this discussion broadens to address grades SA-202 and SA-455.

Figure 22, which shows the corresponding actual yield strength (AYS) for these same steels, illustrates the interrelationship in part – wherein it is evident that the apparent decline in toughness comes at the price of increased strength. This tradeoff between strength and ductility and toughness and the need for both in the same grade of steel led to a fundamental shift in steel-making and processing, which began with high-strength low-alloy steels in the early 1960s and has continued since. It is precisely this circumstance that made the shift from SA-202 to SA-612 possible.

‡ The history of such tanks traces back decades, with other steels involved historically. Anecdotal data indicate that about 85% of the tanks in current service involve SA-612 in somewhat larger proportion than SA-202. Other grades such as SA-455 and others also have been used, but as time passes these represent a dwindling fraction of the Bobtail tank population. Because SA-612 is predominant and the Trinity-Signature tank was made of this grade, the ensuing analyses and discussion focuses on this steel. Consideration is given subsequently to SA-202 and the lesser used grade SA-455.

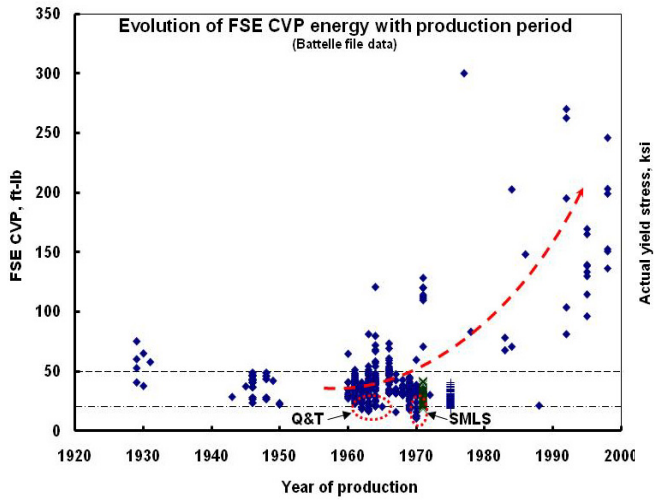

Figure 21. Archival trend in CVN energy

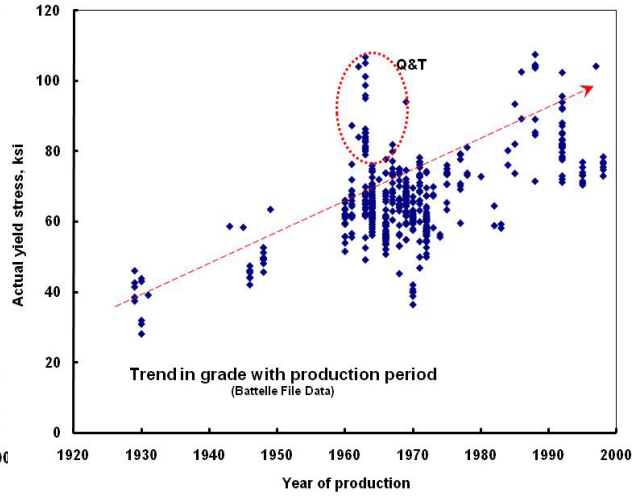

Figure 22. Archival trend in grade

Results – Predicted Failure Boundaries and Leak-Before-Rupture

The above section has presented the selection basis for the parameters that underlie predicting defect growth response at external axial crack-like defects in the bobtail tank, and analysis of leak-before-rupture (LBR). Axial defects represent the worst-case scenario for a cylindrical shell under pressure loading because the hoop stress is twice that of the axial stress. Likewise, crack-like defects are adopted because they represent a worst-case as compared to volumetric or other blunt defects. External defects represent a worst-case as compared to internal defects, as the bulging that can occur for external cracks has a larger influence on growth than does pressure acting to open internal cracks.

Failing crack-sizes as a function of pressure were characterized in terms of total length, L, and physical depth, d, normalized by the wall thickness, t, for a tank taken at 80-inches in diameter with a wall thickness of 0.481-inch, made of Grade SA-612. The outcomes of this specific scenario and others regardless of the grade or tank dimensions are presented in the format of Figure 23 and Figure 24. The circumstances reported in these figures have been chosen to illustrate typical outcomes relative to the effects of toughness, realizing as noted above that the other parameters exert much less influence on these results.

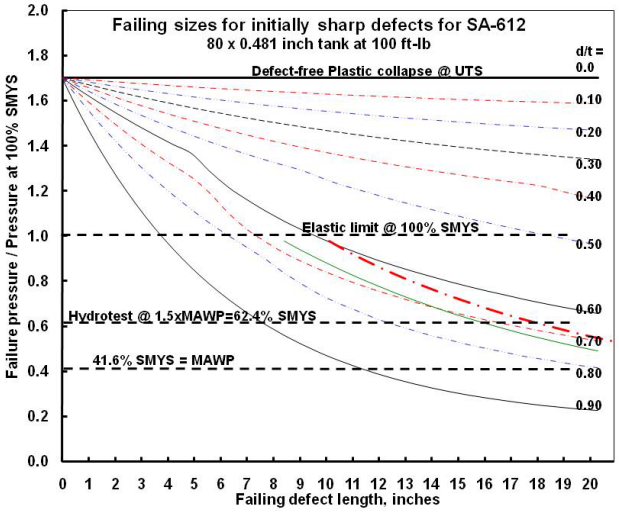

Figure 23. Failure at CVP = 100 ft-lb

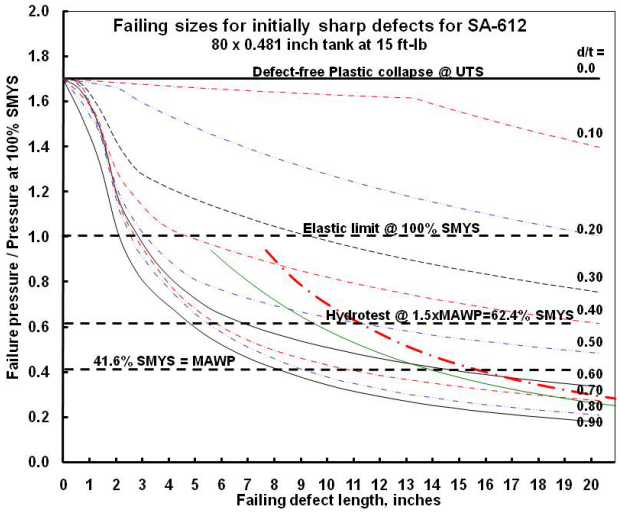

Figure 24. Failure at CVP = 15 ft-lb

Figures 23 and 24 respectively present extremes in toughness – at 100 ft-lb and at 15 ft-lb – with the response at other values above and below these also quantified. The y-axis presents the failure stress (or pressure) normalized by SMYS (or the pressure corresponding to SMYS), the x-axis presents the defect length, L, while the defect depth is represented by the ten contours of constant d/t, which run from the upper left toward the right side of these figures. Two additional contours are shown, which begin just below the horizontal line at a y-axis value of unity, and run down and converge toward the right side of these figures. These converging bounds represent the onset of axial instability and incipient axial instability, and thus define the boundary between leak and rupture. They converge because as the critical defect length increases there is less stable axial growth prior to instability.

Horizontal lines in this format represent constant pressure, with the same four important pressure levels included in each plot. The lowest line represents the service pressure or MAWP, which is 41.6% of SMYS and so falls at a y-axis value of 0.416. The line above that for MAWP reflects the hydrotest pressure, which is 62.4% of SMYS and thus falls at a y-axis value of 0.624. The line above that for the hydrotest pressure represents the limit of elastic response relative to SMYS (not AYS, which in concept exceeds SMYS). By definition this is 100% of SMYS and so falls at a y-axis value of unity. Finally, the topmost line reflects the pressure at plastic collapse and also based on the depth contours represents the failure pressure of a defect-free tank. While the failure pressure of a cylindrical vessel depends on both the strain-hardening exponent and the ultimate tensile stress [Zhu 2007] (which for most distributions of UTS generally exceeds SMTS), for the steels in bobtail tanks this upper bound is reasonably set at the UTS. On this basis, this upper bound is defined by the ratio of the UTS to SMYS, which for the present analysis is about 1.7, such that this upper trend falls at a y-axis value of 1.7.

It is apparent from both Figure 23 and Figure 24 that long very deep defects can survive a hydrotest to the levels mandated for use in the propane cargo tank industry. Increasing the test pressure does not offset the effects of toughness that underlie this response, as very long deep

defects have survived in full-scale testing to pressures in excess of 100% of SMYS [Leis 2001: Appendix 7]. In this context, hydrotesting is ineffective, which underlies the emergence of AIV in the transmission pipeline industry [Leis 2001, Leis 2000, Zhou 2008]. More on this follows after further discussion of the trends in Figures 23 and 24.

Comparing the trends in Figure 23 with those in Figure 24 shows strong differences that trace to the effect of toughness on defect growth. As discussed in more detail in Appendix B, prior to the onset of growth cracks in ductile steels blunt, with the extent of this blunting at the crack tip increasing as the toughness increases. In lower-toughness steels, this blunting is hardly noticeable, whereas in higher-toughness steels significant blunting occurs, with the crack opening visible even without magnification. In lower-toughness steels, cracking initiates and grows stably – with the length and depth, and the shape of the crack front controlling its growth in a manner consistent with the toughness that resists its growth and imposed loading that drives its growth according to fracture mechanics theory, which is referred to as "fracture control". As the toughness increases, the growth and stability of the cracking become insensitive to toughness. With this shift, crack advance driven as above by the imposed loading and now resisted by the flow properties of the steel and the remaining net-section, which is referred to as "(plastic) collapse control".

Thus, successful prediction of the failure boundaries and LBR for a bobtail tank requires viable prediction of both collapse and fracture control, with failure occurring between these predictions determined by the lowest of the predicted pressures. As becomes evident in the next section, both collapse and fracture control can be discriminated within the predicted failure boundaries in Figures 23 and 24.

Trends in Failure Controlled by Collapse versus Toughness

Trends that reflect plastic collapse control of failure for sharp defects are smooth and continuous, and are uniformly "nested" as a function of defect depth (equally net section), with the trend for a given depth being independent of toughness. This can be seen in reference to Figure 23 in the failure boundaries for all depths up through d/t = 0.50. In general these trends are smooth and continuous, with failure pressure decreasing uniformly as depth increases. But, even for these trends close examination indicates a "break" occurs in the results for d/t = 0.40 at a length of about 18-inches, with a more subtle break also occurs in the results for d/t = 0.50 at a length of about 9-inches. These breaks indicate the transition from collapse control to fracture control, which occurs at a lower pressure than occurs if collapse controlled. Examination of the other trends in this figure shows that a strong break is evident for d/t = 0.60, while more subtle breaks occur for d/t = 0.70 and 0.80, with a transition back to collapse control for the deeper defects. In general, collapse controls the deeper and shallower defects, with fracture intervening at the intermediate depths [Leis 2001].

At toughness levels the order of 125 ft-lb and above extensive parametric analysis like that shown in Figures 23 and 24 indicates that all failure boundaries are collapse controlled at all depths, for short as well as longer cracks [Leis 2001]. It is noteworthy that in many cases high toughness steel is available without a price penalty, which given the benefits in increased defect sizes at failure opens to significant potential benefits at nominally no cost. In such scenarios, the limit-state for very long cracks is simply determined from the plastic collapse stress and the net

thickness. In such cases, if the collapse stress is taken as the UTS, the hoop stress at failure is (1-d/t) times the UTS. For shorter cracks, the length of the crack also is a factor, which is obvious in reference to the defect-free limit state where the limit state has a constant value for all defect lengths.

Effect of Toughness on Hydrotest Viability

Evaluating a range of toughness levels provides the basis to trend the effects of toughness, which leads to Figures 25 and 26. Figure 25 shows the failing defect length at the hydrotest pressure as a function of toughness, with these lengths increasing significantly when considered relative to the MAWP. It is apparent from this figure that even at lower toughness the cracking remains stable in response to hydrotest pressure. For example, at a lower-end toughness taken as 5 ft-lbs, a crack 90% through the wall (TW) that was also several inches long could survive the hydrotest. The results in Figure 26 indicate such cracking is stable at hydrotest pressures and so would certainly survive that testing to return to service. If a toughness level that is more likely to be encountered such as 10 ft-lb is considered, Figures 25 and 26 indicate that crack lengths now are at least doubled, with a length of about 5-inches existing 90% TW surviving the hydrotest.

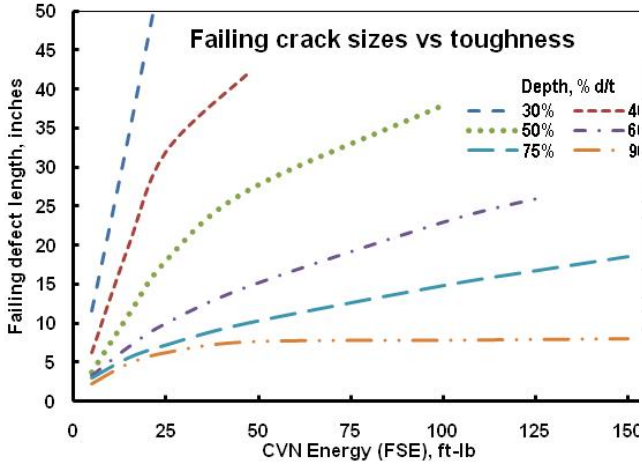

Figure 25. Failing lengths vs CVN energy

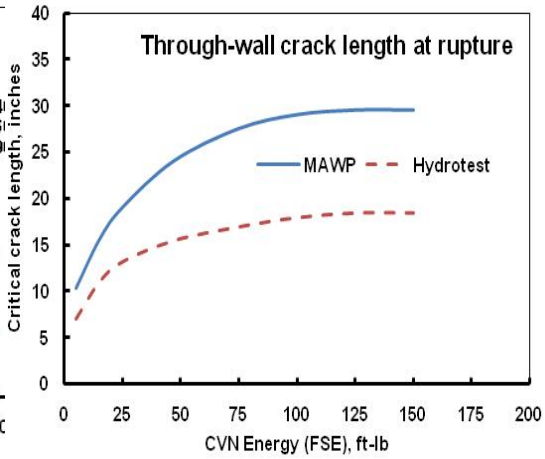

Figure 26. LBR length vs CVN energy

If toughness more typical of modern tanks steels is considered, what was a marginally ineffective hydrotest at worst-case levels becomes clearly ineffective. Consider in this context CVN data developed for samples of SA-612 steel tested by a bobtail tank supplier during his routine qualification process [Mississippi Tank Co. 2005]. Such data for sampling in the weld heat-affected zone (HAZ) from testing done at -55F showed an average toughness of 18 ft-lb. Comparable sampling in the HAZ for testing done at -20F showed values in excess of 60 ft-lb on occasion. In reference to a value of 20 ft-lb, Figures 25 and 26 indicate proportionally longer defects are associated with a 90% TW crack. If instead of such deep cracking a depth of "just" 60% TW was considered, the length of the surviving stable crack increases to 10-inches. As such, tanks can enter the shop for their 5-year hydrotest with rather long and deep cracks and leave with those same cracks. But while that shop visit for a hydrotest will not expose such cracks, because those cracked surfaces will rust due through exposure to rain or even humidity, creating a significant rust stain, it is likely someone in the shop or otherwise will spot that stain long before the tank makes it scheduled visit.

Other CVN data have been developed by sampling steel obtained from the disks removed to create the man-ways [Bowser-Morner 2006]. As this sample excluded a HAZ, regardless of the test temperature the base-metal toughness was anticipated to be much higher. Such results gave rise to levels well above 125 ft-lb, indicating that unstable cracking the body of the tank was not a concern, such that the AIV should focus on axially oriented weld seams – specifically along the weldpad as discussed above.

It follows in regard to these analyses for the SA-612 bobtail tank that even for lower toughness scenarios the periodic hydrotest as it is now mandated brings marginal to no value, as it does not expose quite long and deep defects. Higher toughness further reduces this already marginal value, with significant (deep) cracks several inches in length surviving this periodic testing. More frequent hydrotesting is not an answer, as it does not offset the effects of toughness. While higher pressures do expose smaller cracks, even tests to beyond 100% SMYS are ineffective at higher toughness levels. Significantly, all of the above scenarios showed LBR, which diminishes the utility of the hydrotest but ensure safety until such cracking is visually or otherwise identified.

Amount of Crack Opening for Stable Cracking

The above results suggest that visual inspection might be viable, particularly where the open crack is decorated by a rust stain. While the earlier sections of this report indicate relatively slow crack growth due to in-service cycling, which suggests plenty of time for rust decoration, the question of visual identification absent a rust stain remains. Figure 27 provides insight into this question, where in a first-order fracture-mechanics based estimate of crack mouth opening displacement (CMOD) is shown as a function of normalized crack depth.

Figure 27 reflects the CMOD of a crack whose length is large compared to its depth plotted on the y-axis as a function of normalized crack depth shown on the x-axis. This outcome represents a linear-elastic fracture mechanics estimate that excludes any provision for plastic zone, which would increase the calculated opening. It is apparent from Figure 27 that at the depths discussed above in regard to the utility of periodic hydrotesting that the crack develops significant opening at the surface of the tank. While this calculation would have to be refined to precisely quantify the amount of this opening, this first-order calculation suffices to indicate such cracks would be apparent to the unaided eye.

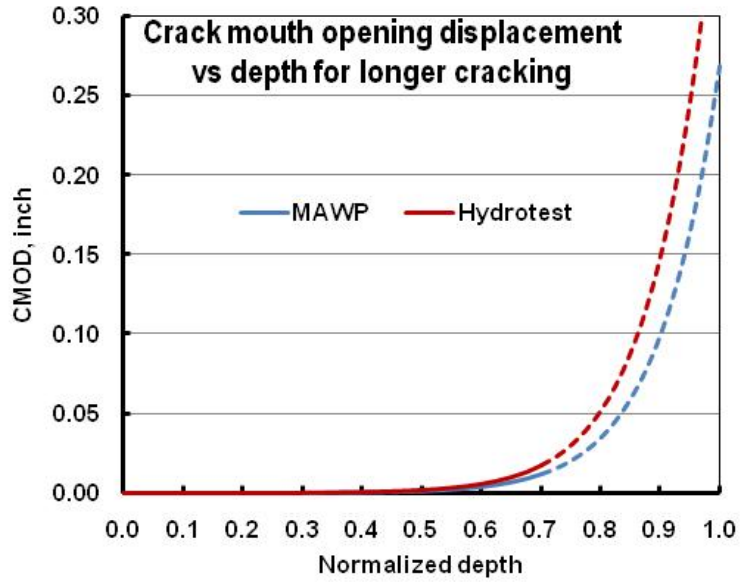

Figure 27. CMOD vs normalized crack depth

Consideration of Grades other than SA-612

To this juncture the focus has been on SA-612, which is the steel currently favored for bobtail tanks, and anecdotal data suggest is now the most prevalent grade in use. As noted earlier, SA-202 was in common use prior to the shift to SA-612, while grades such as SA-455 and others have also been used. While the above outcomes were developed with a view to parametric consideration of toughness, this was done specific to SA-612 against a background of modern steel production wherein the concern for achieving higher toughness is a factor in the selection of steel chemistry and processing.

The realization that toughness is an essential property for steels used in pressure-containing systems became evident in the gas transmission industry, wherein high toughness emerged as the means to control the threat of running ductile fracture. Figure 21 infers this realization came first beginning in the early 1970s, with the benefit that accrues to increased toughness driving the continued push for higher toughness since. As for all changes associated with steel production, the necessary changes in chemistry and processing occurred first in steel mills known to follow "best practices". Reality in this context is that some mills produce better quality and do so more consistently that do other mills. Reality also is that grades that find broad use in applications where high toughness is required tend to be produced with a focus on the properties that make them marketable. It follows that some steels see expanded use depending on price coupled with properties, while production slows or stops for others – just has occurred over time with the shift from SA-202 to SA-612. As time passes, improvements in chemistry and processing continue with a focus on the properties that make the grade marketable. Thus, although the specification for SA-612 tends to be open in regard to chemistry, processing, and the range of the UTS, steel producers do target much tighter levels where it is essential to keep a product competitive with other grades and/or the production of other suppliers. This is evident, for example, in regard to

steel cleanliness, wherein some producers of pressure-vessel steels target sulfur levels as low as 0.001%, in order to achieve toughness levels that keep such grades highly marketable [e.g., ArcelorMittal].

Given the use of the Trinity-Signature bobtail unit made of to SA-612 as typical of such tanks, and the significance of toughness in terms of CVN energy as evident in Figures 23 to 26, it follows that extending the outcome of Figures 25 and 26 to other grades of steel is determined by differences between such grades and SA-612 in regard to factors controlling toughness, and ensuring ductility. As outlined in Appendix D, the literature [e.g., Gray 2009] indicates mechanical measures like the elongation to failure and the UTS are useful metrics, as is steel cleanliness, particularly in regard to very low sulfur content, and the use of calcium treatment to affect shape control of manganese sulfide. It is apparent from Appendix D that none of these metrics support general expansion of the outcomes in Figures 25 and 26 for applications that involve SA-455. A similar conclusion is drawn there for SA-202 in regard to both toughness and elongation – with such being the case except if information was developed under the provisions of the specification's supplemental requirements that demonstrate viable toughness.

While chemistry and related historic trends do not indicate that steels like SA-202 and SA-455 share the same traits as SA-612 produced since it has become the dominant steel used in producing Bobtail tanks, this observation does not preclude their use provided adequate toughness can be demonstrated. Guidance in regard to a minimum toughness follows from analysis of fracture susceptibility, which has been done for SA-202 and SA-455 as used in historic Bobtail tanks in parallel to that as presented for SA-612 in Figures 23 to 27. Such analyses were done assuming the same design expectations as for SA-612, and the same overall tank pressure boundary, except that the wall thickness was increased consistent with the relative values of SMYS for the steels considered. Key in this context is a key trait of fracture mechanics – wherein the driving force for fracture (failure) is strongly dependent on the relative depth of the defect considered. Accordingly, because the thickness of the wall increases inversely with the ratio of the relative values of SMYS, for the same absolute depth of defect in a SA-612 tank the driving force for fracture in the relatively lower-strength grades is less. This acts to offset the potentially reduced toughness that can be anticipated for these earlier vintage tanks relative to the absolute toughness demand inherently met by SA-612 – as detailed in Appendix D. Analysis of the susceptibility to fracture for SA-202 and SA-455 relative to that presented for SA-612 in Figures 23 to 27 thus shows these lower strength grades to be just conservatively represented by the outcomes for SA-612 under the same design expectations as for SA-612. While conservative in that context, the significant differences in the nature of these steels and their production indicates that their toughness remains a concern – for reasons evident in Appendix D.

Guidance on toughness testing requirements for steels used in pressure vessels (ASME VIII Division 2 Part3 Toughness Testing Exemption Curves) indicate that in this guidance that normalized SA-612 qualifies among the few grades identified therein as the toughest steels. In contrast, steels like SA-202 and SA-455 would be grouped in a less robust category. Adopting that guidance, and considering -40°F as the lower-bound temperature of concern for a Bobtail tank (for which the vapor pressure is zero gauge), it is apparent from that guidance that SA-612 satisfied those requirements for such applications without the need for toughness testing. In

contrast, steels like SA-202 and SA-455 require toughness testing to prove fitness for service in regard to that guidance.

While toughness is not a design concern for this ASME guidance for most applications where the pressure is <1000 psi, toughness is the driver in regard to ensuring LBR, which is the basis for the current approach to assess hydro-retest intervals. The key question in that context is – what is the minimum toughness for the present applications involving steels like SA-202 and SA-455?

For present purposes, minimum required toughness has been assessed with respect to the dependence of the vapor pressure versus temperature response for propane. At 0°F the vapor pressure is about 1/10 of the design minimum, while at 32°F it is roughly 1/5 of that level. Because 32°F is a convenient CVN test temperature (ice-water mix), it is a reasonable basis to quantify toughness testing requirements relative to pressure, such that fracture susceptibility of Bobtail tanks has been assessed relative to a pressure set at 1/5 of design. On that basis, a minimum toughness of 10 ft-lb FSE CVN is identified as safely containing very long deep defects whose depth is 90% through-wall, which makes them easy to visually identify (a 90% deep defect gapes open), but still adequately stable. Recognizing that CVN energy shows scatter, the CVN testing must demonstrate 75% shear-area ductility at 32F with an average of 3 or more samples >15 ft-lb FSE, with none less than 10 ft-lb FSE. Successfully meeting these requirements parallels the outcomes evident in Figures 23-27 for steels like SA-202 and SA-455.

Implications of Industry Experience

Circa 2001, the NPGA conducted a survey to determine whether companies that perform the 5-year hydrostatic test requirement had experienced failures and if so whether a significant number had occurred. The results of the survey, which was designed by the University of Alaska to be statistically significant [NPGA 2001], are as follows[§]:

- Total number of Registered Inspectors conducting hydrostatic testing in the United States: 1,050
- Total number of Registered Inspectors that responded to the survey: 203
- Total number of hydrostatic tests performed: 14, 917
- Total number of failures reported: 92, none of which involved the "bobtail" category (cargo tanks having volumes of 3,500 gallons or less)

This outcome is fully consistent with the above analysis.

Aside from this formal survey, an informal polling of industry experts recently sought to update these outcomes. Unfortunately, only anecdotal evidence emerged: one failure was noted [Auxier 2011] that involved a hydrotest leak found in a pre-service test, where a pressed tank-head leaked due to "laminations" in the plate (a plate material defect). There were no reports of a warranty claim due to a leak, nor were there failures found via hydro retesting. Again, this outcome is fully consistent with the above analysis. A review of PHMSA's Incident Database [US DOT PHMSA] indicates no tank failures in the past ten years that were specifically vessel failures (i.e., not related to fire, traffic accidents, filling from or to another vessel, etc.).

[§] Details of the sample of tanks represented by this survey are unknown to Battelle, aside from inference from the reported conclusions that the responses covered bobtail and other types of tanks.

Alternative Integrity Verification

In view of Figures 25 and 26 for SA-612, and the parallel expectations via minimum toughness testing for SA-202 and SA-455, periodic hydrotesting at the level mandated by the PHMSA is an ineffective measure to ensure the integrity of the typical bobtail tank. Consequently, some form of AIV is required. Based on the ability of a bobtail tank to contain large deep crack, their leak-before-rupture behavior, and the visibility of such cracking if in the field of view, a targeted visual inspection directed at the tank-mounting weld and at other highly stressed sites is a viable and conservative AIV practice.

7. SUMMARY AND CONCLUSION

Analysis has been done to quantify the response of axial defects to pressure under conditions typical of bobtail tanks, with consideration of leak-before-rupture and the extent of the crack opening visible at the tank surface. Based on the results and discussion above one can conclude that:

1. hydrotesting does not expose even large deep defects, so some form of alternative integrity verification is needed;
2. such defects are stable such that the vessel would leak before a catastrophic rupture occurs.

Therefore, a crack will be visually identifiable, based on the above analyses that present a necessary length of approximately 18 inches, before a leak will occur.

An alternative integrity verification practice that targets visual inspection of the welds, and other highly-stressed areas and done as part of the yearly visual inspection should suffice – such a practice would have found cracking decorated by a rust stain long before the current hydro would.

NPGA has sought to obtain research data that would support an industry recommendation to DOT to extend the requalification period from 5 years to 10 years. Battelle has concluded that the analysis and data generated as part of this study supports such a recommendation for tanks meeting the following requirements:

- In dedicated propane service
- Sized less than 3500 gallons water capacity
- Meeting DOT MC-331 specifications
- Constructed of one or more of the following materials:
    - Non-quenched and tempered (NQT) SA-612 steel
    - Non-quenched and tempered (NQT) SA-202 or SA-455 steels, provided the materials have full-size equivalent (FSE) Charpy-vee notch (CVN) energy test data that demonstrate 75% shear-area ductility at 32F with an average of three or more samples greater than 15 ft-lb FSE, with none less than 10 ft-lb FSE.

8. REFERENCES

49CFR, Part 178, design code requirements.

49CFR, Part 178, Section/Paragraph 337.3: on Structural Integrity Requirements.

49CFR, Part 180, Section 407: on MC330 and MC331 Requirements.

Anderson, T., "Stress intensity and crack opening area solutions for through-wall cracks in cylinders and spheres," Welding Research Council Bulletin, n 478, January 2003, p 1-31.

ASME Boiler and Pressure Vessel Code, Section VIII, American Society of Mechanical Engineers, Three Park Avenue, New York, NY 10016

Auxier, D., private communication with Leis and Osborne, February/March, 2011.

Battelle 2005. Evaluating the Possible Extension of the Propane Cargo Tank Inspection Interval, Phase 0 Project Report, prepared by Battelle for the National Propane Gas Association, Washington, D.C., under funding from the Propane Education & Research Council, Washington, D.C., Docket 11445

Battelle 2007. Evaluating the Possible Extension of the Propane Cargo Tank Inspection Interval, Phase 1 Project Report, prepared by Battelle for the National Propane Gas Association, Washington, D.C., under funding from the Propane Education & Research Council, Washington, D.C., Docket 11445

Bowser-Morner Laboratory Report #10017636 52116 601823-601824 to Battelle, February 2006.

Kastner , W., Rohrich , E., Schmitt , W., and Steinbuch, R., "Critical crack sizes in ductile piping," International Journal of Pressure Vessels and Piping, Volume 9, Issue 3, May 1981, Pages 197-219.

Leis, B. N. and Vereley, R. E., "Quality Control, NDT Offer Alternatives to Hydrotesting," Pipeline and Gas Journal, June 2000.

Leis, B. N., "Hydrostatic Testing Of Transmission Pipelines: When It Is Beneficial and Alternatives When It Is Not", PRCI Report PR3-9523, with Seven Appendices, to Pipeline Research Council International, 2001.

Leis, B. N., Brust, F. W., and Scott, P. M., "Development and Validation of a Ductile Flaw Growth Analysis for Gas Transmission Line Pipe", NG-18 Report No. 193, available as PRCI Report L51543, June 1991: for collapse see Leis, B. N., "Analysis of Defect Response to Pressure," Appendix 2 to Reference 4.

Leis, B. N., et al, "Full-Scale Testing to Validate PAFFC and Develop Data to Assist Evaluating the Benefits of Hydrotesting," Appendix 7 of Reference 4.

MATLAB, data analysis software package, MathWorks, Natick, Massachusetts, U.S.A.

Mississippi Tank Co., "Weld & Mat Spec2001 612.pdf," transmitted by email (original file dated 09-16-09, which was extracted from email attachments from M. S. Foy, November 2005).

Mississippi Tank Co.: Procedure Qualification Record No: A10C101-DOT, archival data, dated 03-19-01, which indicates that Gr70N SA-516 was being used in lieu of SA-612 (extracted from email attachments from M. S. Foy, November 2005).

Mississippi Tank Co: Procedure Qualification Record No: TS4401, archival data, dated 10-21-87, which indicates the occasional use of SA-202 into the later 1980s, (extracted from email attachments from M. S. Foy, November 2005).

NPGA 2001 Survey of Bobtail Owners, (email from NPGA's Bruce Swiecicki to Rod Osborne dated

2/28/2011.

Osborne, R. L., "Evaluating the Possible Extension of the Propane Cargo Tank Inspection Interval: Phase 0," January 2005.

Rogers, Tom: private communication with Tom Forte and Rod Osborne, November 16, 2006.

SA-202 "Standard Specification for Pressure Vessel Plates, Alloy Steel, Chromium-Manganese-Silicon," (Identical with ASTM Specification A202 / A202M – but is no longer an active ASTM standard).

SA-612 "Standard Specification for Pressure Vessel Plates, Carbon Steel, High Strength, for Moderate and Lower Temperature Service," (Identical with ASTM Specification A612 / A612M).

Zhou, Joe; Murray, Alan; and Abes, Jake, "Implementation of Alternative Integrity Validation on a Large Diameter Pipeline Construction Project", Paper IPC2008-64479, Proceedings of IPC2008, 7th International Pipeline Conference, September 29-October 3, 2008, Calgary, Alberta, Canada.

Zhu, X. K. and Leis, B. N., "Average Shear Stress Yield Criterion and its Application to Plastic-Collapse Analysis of Pipelines," I. J, Press, Vessels and Piping, Vol. 83, 2006, pp. 663-671, see also Zhu, X. K. and Leis, B. N., "Theoretical and Numerical Predictions of the Burst Strength of Pipelines," J Press, Vessel Tech, ASME, Volume 129, 2007.

US Department of Transportation Pipeline and Hazardous Materials Safety Administration (US DOT PHMSA) Incident Statistics website: http://phmsa.dot.gov/hazmat/library/data-stats/incidents.

APPENDIX A:
PROPANE CARGO TANK
DATA ACQUISITION AND ANALYSIS

APPENDIX A:
PROPANE CARGO TANK
DATA ACQUISITION AND ANALYSIS

PROJECT DESCRIPTION

In Phase 2 of the Cargo Tank Requalification Period Extension project, the project team considered the effect of over-the-road loading. The evaluation involved using a data acquisition system to gather loading response data from strain gages and accelerometers installed at various locations on the tank and on the truck sprung and un-sprung masses. Data were also gathered at various fill levels and during both continuous driving (road) and discrete event tests. The project team analyzed the data using Battelle-developed algorithms to estimate fatigue and failure metrics.

This appendix describes the sensing, acquisition and analysis system the team used for acquisition and analysis.

TESTING REQUIREMENTS

The data collected to study the response of the tank must be collected when the truck is subjected to loading representative of what is seen during normal truck operation and must include low probability events such as panic braking and extreme road surface irregularities. Hence, data was acquired both during continuous (or road driving) and discrete events (driving over bumps, braking, etc.). The test plan outlined in the test plan, lists the various tests conducted to achieve representative truck loading duty cycles. The testing was carried out at Battelle facilities and on "durability" tracks at the Transportation Research Center (TRC), East Liberty, OH. Initial braking and bump tests were conducted at Battelle facilities (Columbus and West Jefferson, OH).

The locations and orientations of the strain gages and accelerometers were determined from finite element stress analyses of the tank and truck for various simulated loading conditions. This process resulted in a total of 40 candidate strain gage locations and orientations. These tests provided additional guidance for identifying which of the sensors could be eliminated because they did not show significant strains during any of the discrete tests or torture track tests.

SENSING

The purpose of the sensing system was to obtain vehicle strain and load levels during representative loading of the tanker truck. The following sensors were used

1) Strain gages – Initially 60 biaxial Vishay 350 ohm strain gauges in a quarter bridge configuration were applied to the tank (for strain gage measurements to determine stress magnitudes and reversals at welds and other stress concentration points), but only 40 channels were available for data acquisition. Two configurations named 'Alpha' and 'Bravo' were tested with various handling tests to choose the 40 most important strain channels. This final 'Charlie' configuration was used for the bulk of the road tests.

Table 1 shows the "Charlie" configuration. Figures A1 to A7 show the locations of the strain gauges as referenced to weld lines and other notable features of the tank.

2) Accelerometers – The six accelerometers (for capturing sprung mass modes and load levels) were DC coupled Kistler model 8305B50M2, capable of measuring up to +/-50g with a 0-500 Hz frequency range. Calibration curves from the manufacturer were applied to the data. For the Alpha, Bravo, and Charlie configurations, all the mounting locations for the accelerometers were the same as shown in Figure A8. Additionally Figure A9 shows the Delta and Echo configurations, which used the same strain gauge locations as Charlie, but moved the accelerometers to the liquid pump and the rear vapor and liquid flanges.
3) String potentiometers – The five string pots (to measure relative displacements, for example at the suspensions) were used to help correlate with gross vehicle events such as going over bumps, and turning. The string pots were used as follows: one near each wheel to measure suspension travel, and one on the steering linkage to measure steering displacement.
4) Miscellaneous sensors – (these included a speed sensor and a pressure transducer – to provide vehicle status information).
5) Video – The test events and routes were videotaped for later review and correlation with the data

As mentioned above, due to the large number of strain gages, they could not be recorded simultaneously; therefore, two groupings (named 'Alpha' and 'Bravo') of the strain gages were initially used to obtain the baseline data. The response of the various strain gages was observed during road driving and on the torture tracks as well as discrete events, which included braking tests, bump tests, slalom, and constant radius turning tests. The final configuration 'Charlie' of the sensors locations were based on the results of the analysis of this data.

Table 1. Transducer strain gage assignments.

Strain Transducer	Location	Orientation Relative to Weld	Number of Gages
1	Gusset Tab, Front	Normal	2
2	Gusset Tab, Front	Tangent	2
3	Opposite Gusset Tab, Front	Normal	2
4	Opposite Gusset Tab, Front	Tangent	2
5	Doubler End, Front	Normal	2
6	Doubler End, Front	Tangent	2
7	Head Weld, Front	Normal	2
8	Head Weld, Front	Tangent	2
9	Gusset Tab, Rear	Normal	2
10	Gusset Tab, Rear	Tangent	2
11	Doubler End, Rear	Normal	2
12	Doubler End, Rear	Tangent	2
13	Head Weld, Rear	Normal	2
14	Head Weld, Rear	Tangent	2
15	Gusset Tab, Center	Normal	2

Strain Transducer	Location	Orientation Relative to Weld	Number of Gages
16	Gusset Tab, Center	Tangent	2
17	Manway	Normal	2
18	Manway	Tangent	2
19	Pump Flange, Front	Normal	2
20	Pump Flange, Front	Tangent	2
21	Pump Flange, Side	Normal	2
22	Pump Flange, Side	Tangent	2
23	Longitudinal Seam	Normal	2
24	Longitudinal Seam	Tangent	2
25	Head at Longitudinal Seam	Normal	2
26	Head at Longitudinal Seam	Tangent	2
27	Baffle Pad, Longitudinal Weld	Normal	1
28	Baffle Pad, Longitudinal Weld	Normal	1
29	Baffle Pad, Longitudinal Weld	Tangent	1
30	Baffle Pad, Longitudinal Weld	Tangent	1
31	Baffle Pad, Circumferential Weld	Normal	1
32	Baffle Pad, Circumferential Weld	Normal	1
33	Baffle Pad, Circumferential Weld	Tangent	1
34	Baffle Pad, Circumferential Weld	Tangent	1

DATA ACQUISITION HARDWARE

A National Instruments data acquisition chassis, NI cDAQ-9172[1], was used to acquire the data from the sensors. This chassis supports multi-sensor accelerometer, strain gage and thermocouple modules for acquiring the relevant data. The NI DAQ-9172 is an 8-slot NI CompactDAQ chassis that can hold up to eight C Series I/O modules. Dedicated C series modules were purchased to acquire strain, acceleration, and temperature data. In addition to this, generic, C-series modules for acquiring analog voltages were also purchased. Each of these modules can acquire multiple channels of data. The NI cDAQ-9172 is a USB 2.0-compliant device and the data can thus be easily transferred from the DAQ hardware to the software for storage and analysis.

[1] National Instruments cDAQ-9172, http://sine.ni.com/nips/cds/view/p/lang/en/nid/202545.

Figure A1. National Instruments Data Acquisition Hardware, cDAQ-9172

During the tests it was envisioned that time responses of about 60 channels of data were likely to be required for each test. Hence, two NI-DAQ 9172 chasses were acquired. National Instruments provides the capability of synchronizing the data collection between the two chasses both in hardware and software.

DATA ACQUISITON AND ANALYSIS SOFTWARE SYSTEM DESCRIPTION

The software system was used to acquire and analyze the data that the team collected during representative loading scenarios of the tanker truck system. The fatigue and failure estimation analysis was done offline and did not require a real-time implementation. However, other analysis and data display was necessary when the data was acquired. The system is divided into acquisition and analysis subsystems

A vendor, Real-Time Innovations (RTI), developed a test harness based on RTI's software package *Constellation*, to acquire data from the National Instruments hardware. *Constellation*, is a graphical-based software development platform, to rapidly develop an interchangeable suite of hardware/software components.

Test Harness Architecture

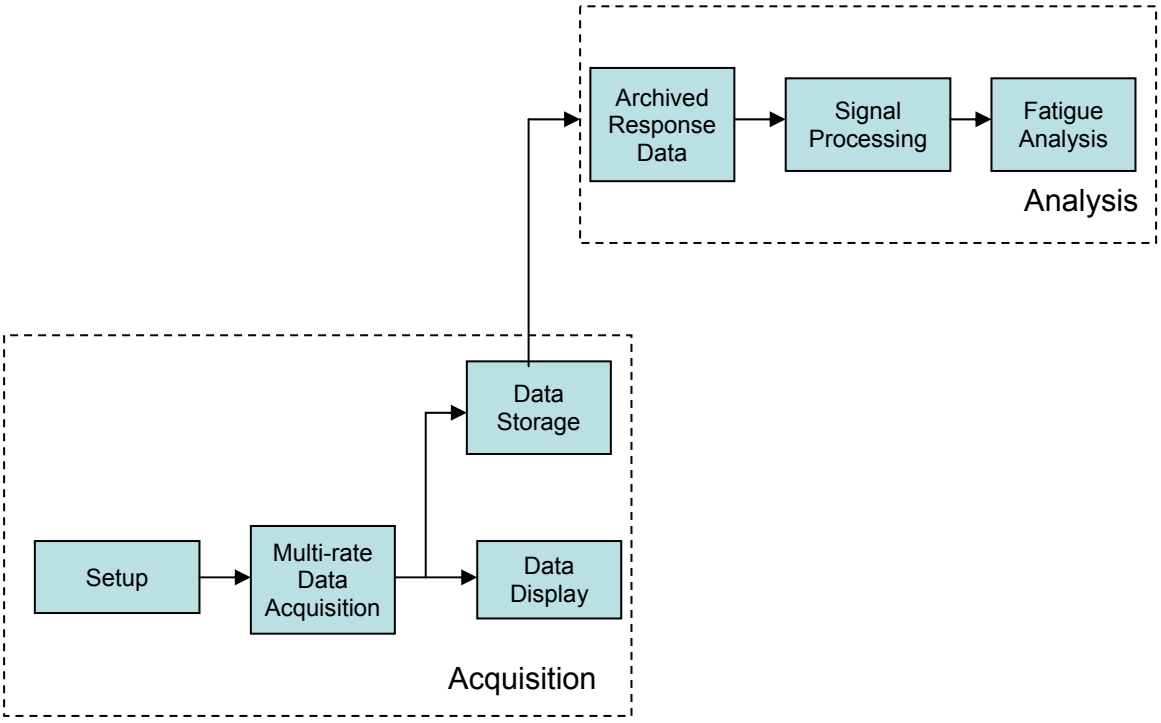

Figure A2. Software system for data acquisition and analysis of PNG tanker truck test

The system is divided into two main subsystems as shown in Figure 2. These include data the acquisition and analysis subsystems. The next few sections deal with the detailed design specification and in particular with how the data acquisition software is implemented in *Constellation*.

Data Acquisition System

National Instruments provides a software environment, LabView, with a Measurement explorer for building NI hardware based data acquisition system. In this project, we used Constellation for data acquisition. The Constellation approach provides an open architecture approach to developing an acquisition system that can include other third party hardware and analysis libraries. This gives the developer the freedom of adding non-NI hardware and provides a platform to easily reconfigure the system to interface with this hardware with minimal alterations to the analysis part of the software.

Data was acquired at sampling rates of approximately 3,846 Hz and 2,000 Hz. The sampling rate is dependent on the data acquisition modules used. Depending on the modules, the actual achievable sampling rate is determined and set in the NI cDAQ 9172 hardware. High frequency data in this application is only required if one wants to study events that result in bottoming out

of suspensions and contact with suspension stops. Heavy-vehicle vibration modes due to tire-road interaction are as below[2].

- 1.5-4 Hz – body (sprung mass) bounce, pitch and roll vibration modes
- 8-15 Hz – un-sprung mass bounce and roll, suspension pitch modes.

Even so, data was collected at the high frequencies to determine loading and detect any high frequency response.

The NIDAQmx programming environment provides an interface with the data acquisition system. The DAQmx comes with a set of Application Programming Interfaces (APIs) required for data acquisition programming. The DAQmx API is simply a set of libraries containing functions on how to perform all the data acquisition operations such as analog input, analog output, Counter and Digital Input/Output. These APIs include support for LabWindows CVI, C, C++, Visual Basic 6.0,VB.NET and C#.

The Battelle implementation of the *Constellation* data acquisition system consists of *Constellation* components that make use of these APIs for acquiring data. Specifically, the API's are used for the following:

- Create a task and virtual channels
- Configure the timing parameters
- Start the task
- Perform read operations from the DAQ
- Stop and clear the task.

The following paragraphs outline the *Constellation* data flow components (DFCs) for Data Acquisition and the APIs used for each task.

1) Task and Channel Initialization: A task in NI consists of one or multiple virtual channels of data. Each virtual channel is the representation in software for a physical channel on the device. For example, all the strain gage channels can be grouped under a single "Strain Measurement" task. Similarly, one could group all measurement data from a particular location in a task named, say, "RearLeftLeafspring" task.

This DFC performs three main functions:

1) Create all the tasks
2) Define the virtual channels that comprise these tasks
3) Define sampling rates for each of these tasks.

The DFC calls these APIs only once in an acquisition cycle since this initialization takes place only once during the data acquisition task.

[2] Hassan, R., McManus, K., "Estimating dynamic loading of pavements from surface profile properties," Road and Transportation Research, September 2001.

2) Data Acquisition Task: The actual data acquisition does not start or stop automatically after a task has been defined. The relevant task is to be started for data acquisition to start. Similarly, the task is stopped to stop data acquisition. Lastly, a task must be cleared to clear all buffers and release memory for other tasks.

This DFC performs three functions

1) Starting a task – initiating data acquisition
2) Reads the data – reads the channel information and stores it in a buffer.
3) Stops and clears task – stops data acquisition, de-allocates resources.

Data Analysis

The acquired data will be analyzed to predict lifecycle estimates for the tanker-truck. Processing of the data will mainly be done from collected data files.

1) Data Storage - The data storage involves storing the data in a format suitable for processing by the fatigue analysis software. Components were defined in Constellation to facilitate both ASCII and binary data storage. The latter is especially useful for collecting data during continuous (road driving) tests. During such tests data was acquired in 5-10 minute segments and the real time storage requirements for acquired data is both CPU and memory intensive, thus necessitating binary storage of data.

2) Signal processing – Standard signal processing included determining strain gage cycle reversals, statistical characteristics of strain gage data, low pass filtering.

3) Fatigue analysis – Currently all the fatigue analysis will be done using Battelle legacy code. Some of the preliminary analysis will be done in *Constellation* DFCs and stored in a format suitable for further processing.

4) Data Display – Data was monitored during data collection. This was done to ensure that all sensors were functioning and to also observe and verify the tanker response to different levels of loading. The software provided the flexibility of viewing data with *Constellation's* Scope functionality. In, addition data display capability was also provided in MATLAB. The MATLAB based program created for this program allows the user to view one, a few or all channels of data simultaneously. Data can be presented to the viewer in time or frequency domain.

There is no separately defined user interface. Data acquisition was initiated from the *Constellation* Application level.

CONCLUSIONS

The test harness was used to collect the data both during discrete event and longer road driving events. The data was examined during testing to ensure that the data being collected was indeed reasonable. MATLAB-based software was used for plotting and examining the data. The initial

brake and bump tests allowed the team to select appropriate locations for placement of strain gages and accelerometers.

The Constellation approach favors reusability and ease of reconfigurability. Constellation-based application also provides a scalable platform. The designed test harness can be easily modified to account for increase in the number and type of sensors as well as any changes in the data acquisition system. Addition of more analysis functionality is easy. The software can be reused for similar acquisition and analysis programs.

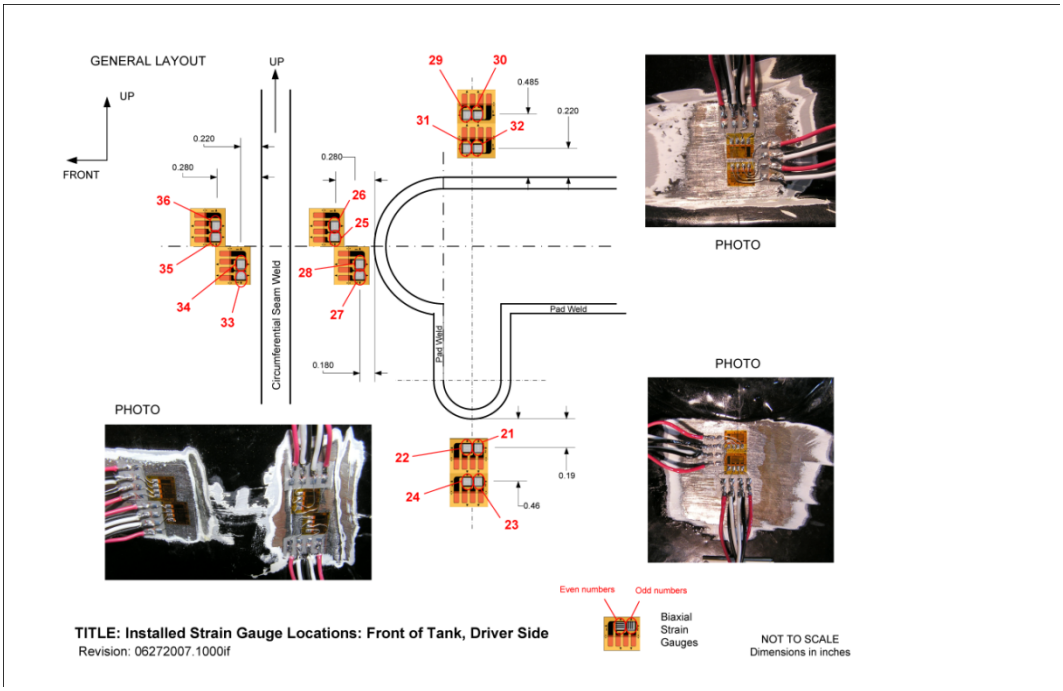

Figure A2. Strain gauge installation – Tank front, driver's side

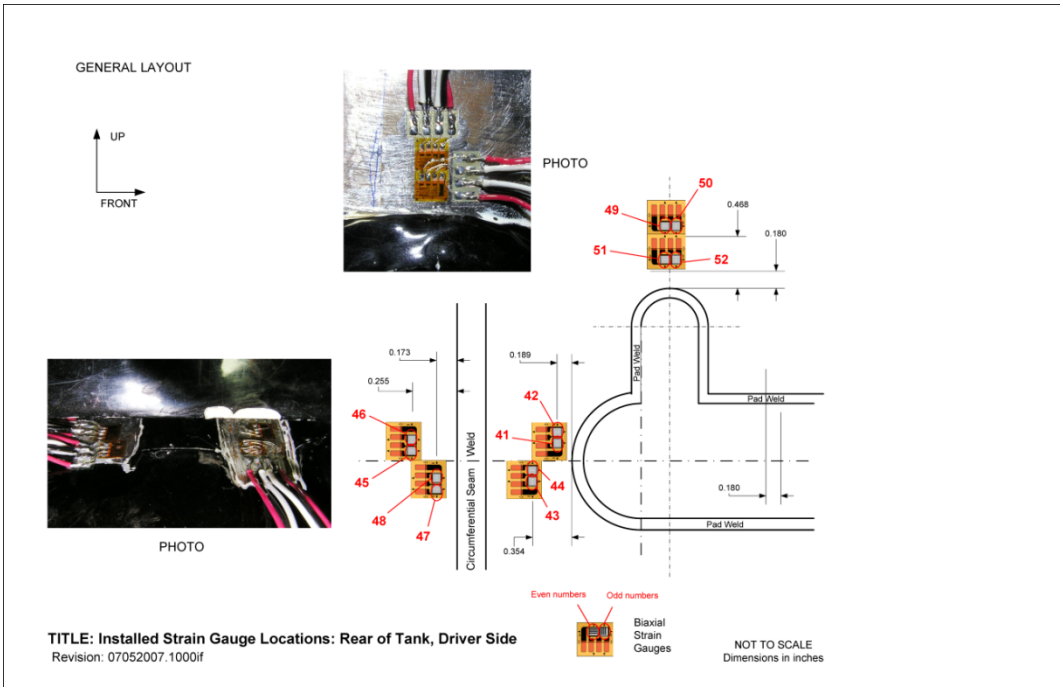

Figure A3. Strain gauge installation – Tank rear, driver's side

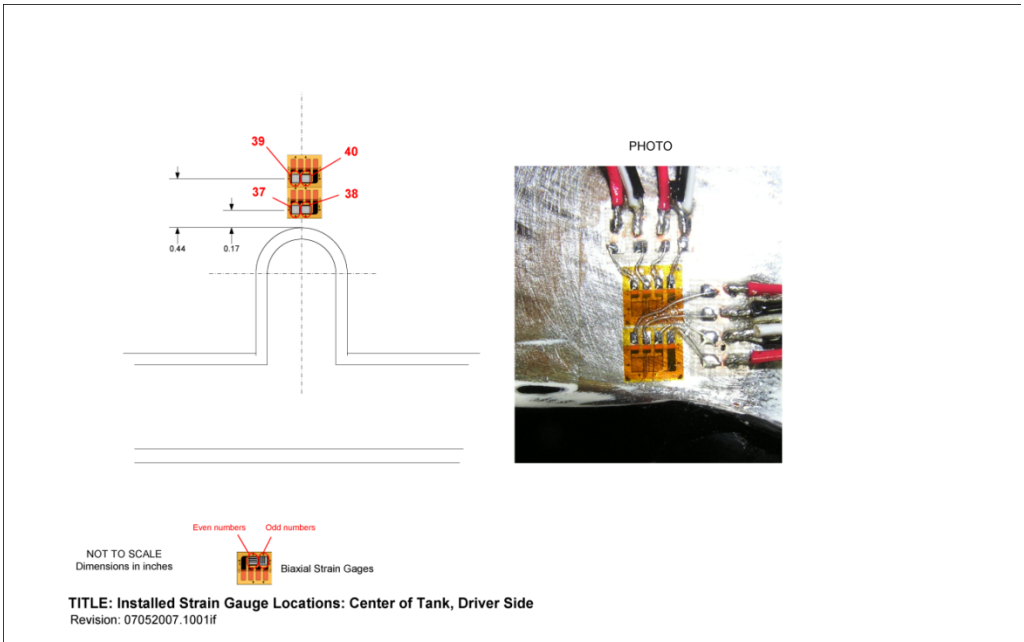

Figure A4. Strain gauge installation – Tank center, driver's side

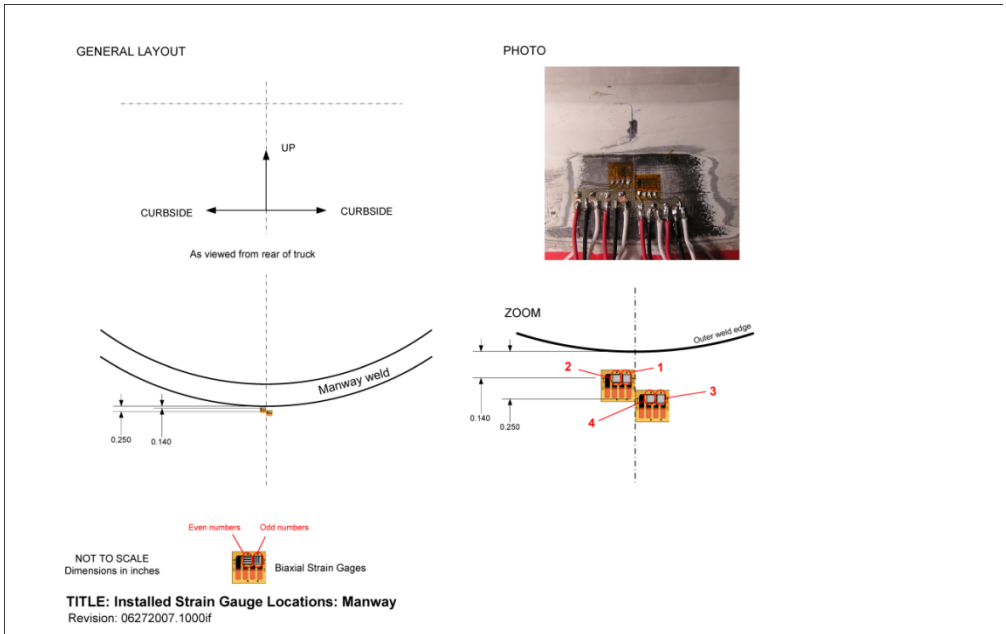

Figure A5. Strain gauge installation – Tank manway

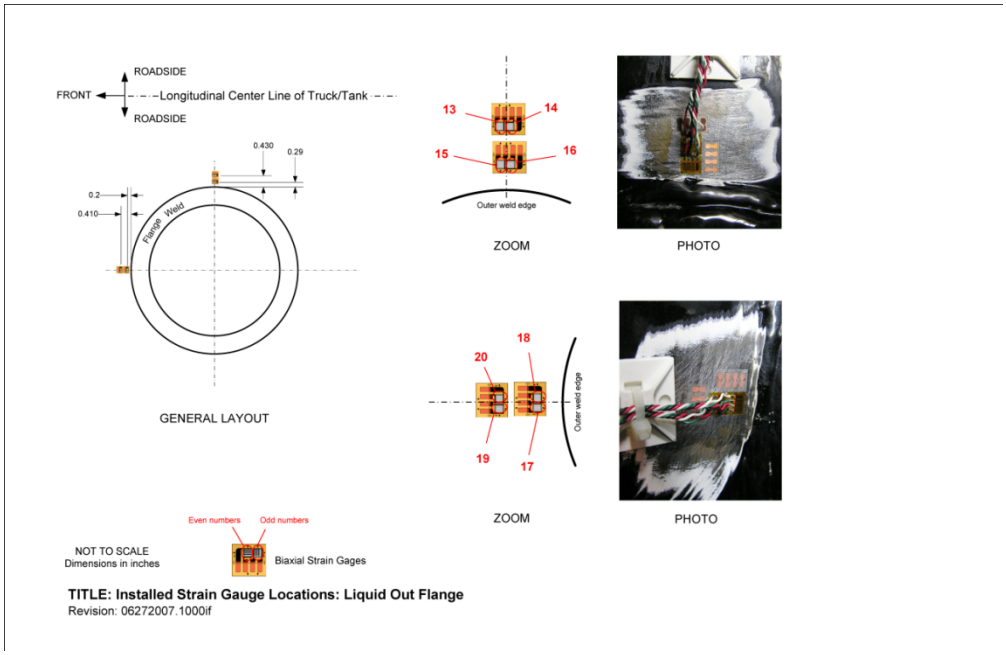

Figure A6. Strain gauge installation – Tank liquid outlet flange

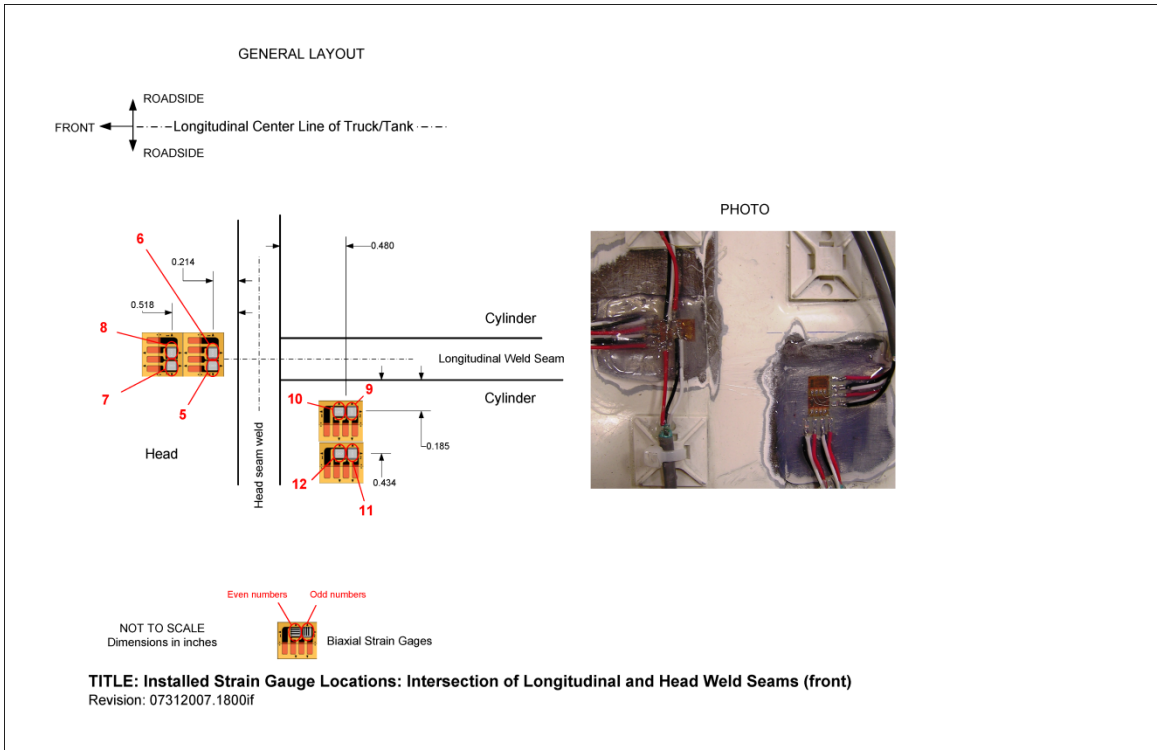

Figure A7. Strain gauge installation – Tank weld seam intersection (front head and longitudinal)

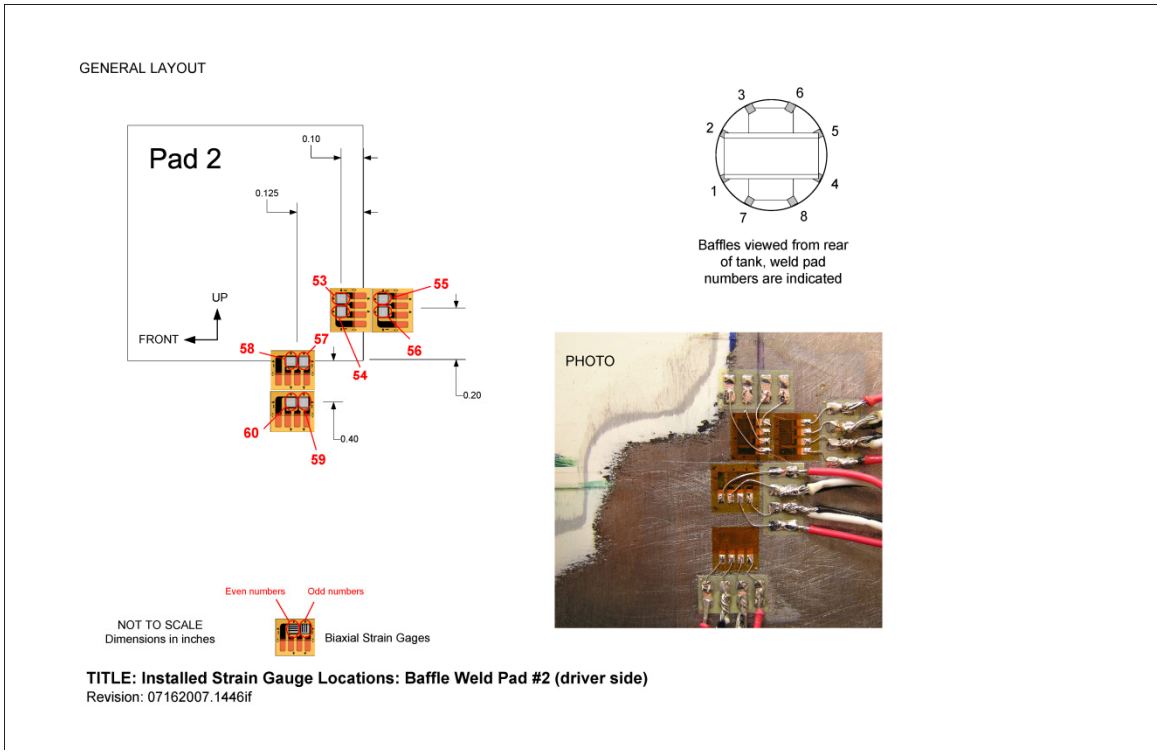

Figure A8. Strain gauge installation – Tank baffle weld pad, driver's side

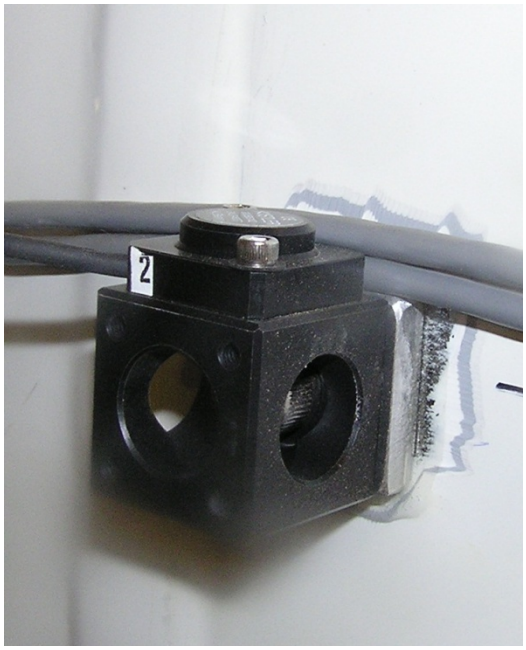

Figure A9. Accelerometer installation on tank midplane, representative of Charlie configuration

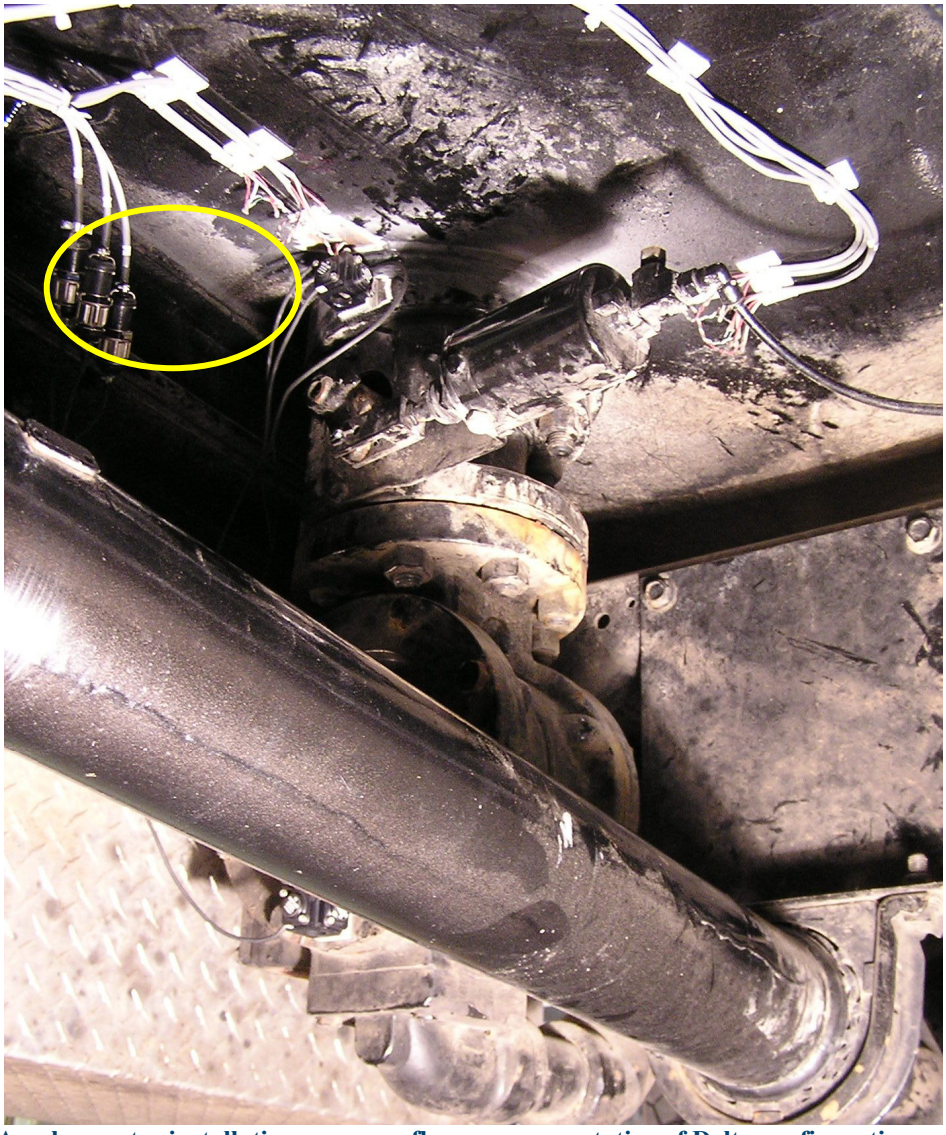

Figure A10. Accelerometer installation on pump flange, representative of Delta configuration

APPENDIX B:
OVERVIEW OF DEFECT RESPONSE TO PRESSURE AND LEAK-BEFORE-RUPTURE

APPENDIX B:
OVERVIEW OF DEFECT RESPONSE TO PRESSURE AND LEAK-BEFORE-RUPTURE

BACKGROUND

Appendix A has used technology to predict defect response to pressure and whether leak-before-rupture (LBR) occurs without details to support these aspects. This expedient was adopted under the expectation that most NPGA readers were interested first in outcomes relevant to hydro-retesting, and then as needed would consider the underlying process and technology. This appendix fills the gaps that remain: first the process associated with defect growth driven by pressure is summarized, and then the technology developed to characterize that process is outlined.

Defect Response to Pressure and Leak-Before-Rupture

Consider first generic discussion of crack growth via stable tearing for ductile steels and the cracking response as observed in experiments that characterize this behavior under gradually increasing pressure to failure (the so-called "burst test"). Thereafter this generic response is discussed in regard to tougher steels, whose behavior is then contrasted to moderate and lower-toughness steels. While time-dependent cracking also can occur, such is not particularly important to the hydrotest response of a Bobtail tank, and so is largely ignored hereafter.

Fracture Resistance to Crack Growth via Stable Tearing

Tests used to characterize the stable crack extension and the eventual failure of a material tend to depend on 1) the testing practices available when concern for fracture response emerges, 2) the nature of the material's fracture response, and 3) the nature of the loadings that might promote failure. For these reasons, quasi-static as well as dynamic test methods evolved to quantify fracture resistance under both extremes of loading rate, and as time passed and materials became more resistant to fracture, new methods evolved to characterize this increased resistance.

Current testing practices used in the pressure vessel and pipeline industry now use J-Resistance (J-R) testing[B1] to quantify the resistance of the steel to the initiation and growth of cracking. Likewise, as ductile response is now sought at lower temperatures (to avoid concern for brittle fracture), the testing practices developed to quantify fracture resistance were focused on increased ductile resistance. Because these historic testing and related practices are well known in the pressure vessel and pipeline industry while newer methods to develop J-R curves are less known, this section focuses on testing to quantify stable tearing and tearing instability as these processes develop in high-toughness materials. Following this, background to nonlinear fracture mechanics (NLFM) concepts is presented for readers new to such methods. As this discussion is specific to the ductile flaw-growth model (DFGM), readers interested in further discussion should consult one of the many textbooks on fracture mechanics[e.g., B2].

The fracture resistance of high-toughness line-pipe steels is well characterized by the J-R curve which is developed according to test methods such as ASTM E1820[B1] and the related NLFM

concepts. While other practices have evolved for this purpose, use of E1820 is clearly preferred. This practice suitably reflects the blunting response typical of tougher steels. It characterizes plane strain circumstances when related criteria are satisfied, whereas the practice should be used with the full-pipe-wall-thickness when characterizing plane stress response. The effects of differing levels of constraint between the test and the application should be addressed with an appropriate constraint parameter[e.g., see B3], particularly in regard to assessing initiation resistance.

The effects of increased toughness as develops for higher-toughness line-pipe steels are clearly evident in the response of a defect to increasing pressure, which is considered next in the context of the schematic of this process shown in Figure B1. In this schematic, the x-axis is a measure of defect growth into the wall thickness, normalized by the wall thickness. The y-axis in Figure B1 is failure pressure, which is directly proportional to the hoop stress at failure and normalized by the pressure corresponding to defect free pipe. Full-scale tests on pipe indicate the defect-free failure stress for many typically used steels is nominally the ultimate tensile stress (UTS), although in general the strain-hardening exponent is also a factor[B4]. This means the maximum pressure encountered on the y-axis corresponds to this stress level, as was noted in regard to Appendix A in reference to Figures A3 and A4. For the sake of illustration the schematic in Figure B1 considers the case of a defect whose initial depth prior to the pressure test was ~40-percent of the wall thickness.

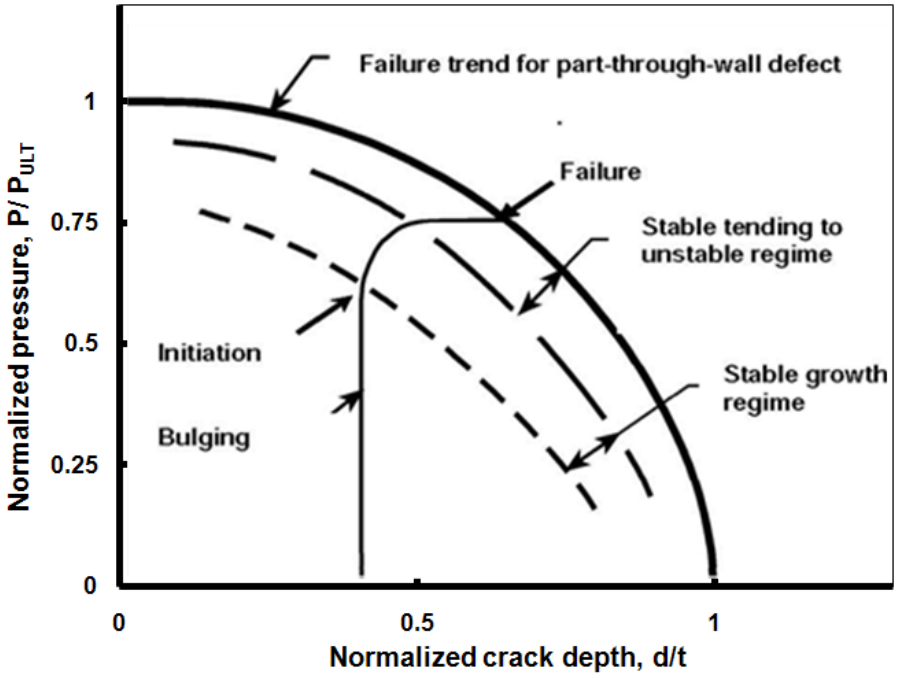

Figure B1. Schematic of pressure-driven defect-growth response at axial external defects

Defect Response to Increasing Pressure

Experimental studies reported in the literature[e.g., B5-B7] indicate that axial defects in a pressure vessel or pipeline grow under pressure through the wall in a three-step failure process according to the schematic introduced above in Figure B1. This figure reflects the effects of both plastic collapse and fracture on the failure behavior on axial part-through-wall (PTW) defects, being labeled for and reflecting the response typical of tougher materials. As becomes evident in the

ensuing text, higher toughness simply affects greater tolerance for stable defect growth, which means that Figure B1 also embeds the response of less-tough materials. Logically, differences in defect tolerance affected by toughness are evident in the extent of stable extension in the context of Figure B1.

Full-scale experiments indicate the first step in the failure process of an axially oriented defect is gradual bulging of the vessel or pipe local to the defect as the pressure is increased. Bulging develops increases as the pressure increases that for tougher steels can occur without significant defect growth. Bulging that develops without crack growth occurs along the vertical line shown in Figure B1 – which is vertical because the pressure increases absent crack extension.

For ductile thin-wall pipe and deep defects, bulging can be noticeable to the unaided eye, but for heavier-wall pipe, shallow defects, or lower toughness steels, relatively less bulging occurs prior to failure. It is noteworthy that the bulging of concern is that developing prior to instability, which is typically much reduced from the bulge that develops following the energy released with instability – which in some cases can result in a quite large local pucker along the wall.

The second step in the failure of axial PTW defects involves the nucleation of cracking and its possible stable extension into the wall and along the pipe. This cracking continues as the pressure increases where time independent cracking occurs, with growth ceasing immediately when the pressure stops increasing. In contrast, when time dependent response occurs crack growth can continue even though the external loading ceases.

The third and final step in the failure of axial PTW defects involves initially stable time dependent crack extension at constant pressure, which eventually transitions to unstable crack growth, and rapid penetration into and through the wall thickness.

Whether the breach created in pipe wall as the PTW crack transitions through-wall (TW) leads to a leak or a rupture (and fracture propagation along the length of the pipe) depends on the length of the break, the geometry of the line pipe and its mechanical and fracture properties, and the properties of the pressurizing media. Very short splits are likely when very tough steels are involved, whereas longer splits occur as the toughness decreases.

Stable crack extension with increasing load absent time-dependent effects is shown as the curved segment labeled such in Figure B1. In general, stable extension also can include a time dependent component that reflects stress-activated creep[B7,B8], with significant extension indicated possible at constant test pressure in cases where the wall stress is locally high[B7,B8]. However, because the hydrotest pressure is relatively low compared to SMYS, little such response would occur for in Bobtail tank applications such that this aspect is not of importance hereafter.

Cracking Response Characteristic of Higher-Toughness Materials

Higher toughness materials are broadly available for more than a decade, where higher toughness for present purposes is taken as toughness greater or equal that 125 ft-lb full-size equivalent (FSE) Charpy-vee notch (CVN) energy[e.g., B9]. Such materials undergo extensive blunting along their initially sharp crack front, which makes them very resistant to fracture. In the same way

tough steels blunt initially sharp cracks, their growth involves the extension along a blunted crack-tip. For these reasons, such steels are very fracture tolerant and can suffer significant stable crack extension as compared to moderate or much-less-tough steels, and show significant bulging prior to failure in high diameter-to-thickness (D/t) situations. In contrast, stress-state and loading induced constraint along such cracks can alter the apparent resistance to fracture of tough steels.

For such steels, failure occurs after stable tearing that can include significant cold creep for an extended period. In reference to Figure B1 this behavior occurs at constant pressure such that this response develops along a horizontal (pressure independent) segment. This segment is labeled as "stable tending to unstable" in Figure B1. Such response is preceded by pressure dependent cracking that occurs throughout the regime labeled "stable" in Figure B1. Increased toughness or conditions more favorable to plane stress lead to failure at relatively higher pressures, which can involve correspondingly larger amounts of extension. An upper-bound toughness exists beyond which failure pressure ceases to increase as toughness increases. As alluded to briefly in Appendix A, this signals the transition from toughness-controlled failure to plastic-collapse-controlled failure. Plastic-collapse-controlled failures are sometimes termed "flow-stress dependent" failures in spite of the fact that "plastic collapse" actually occurs locally at the UTS, or close to it depending primarily on local state of stress[B4,B10-B13].

At toughness levels less that that indicated above the extent of the blunting diminishes, as does the propensity and duration of cold creep. But, so long as the deformations and cracking processes remain ductile the behavior at the crack tip remains similar, as becomes apparent in the next section. While little has been said here about time dependent stable tearing, simulations do point to cases where time-dependent cracking can be a significant practical consideration[B14].

Response to Increasing Pressure in Less-Tough Steels, and Low-Shear Area

Less tough steels exhibit the same tendencies shown in Figure B1, except the extent decreases as toughness decreases. This is clear, for example, in comparing results Reference B9 to those in Reference B7, where it is apparent that for burst pressure experiments on one higher toughness steel (toughness > 100 ft-lb) there was significant extension into the crack depth and along the wall, with amounts measured more than five times that for a moderate toughness-steel (30 ft-lb). The effects of pressure as well as evidence of time dependent cracking are apparent in these trends. Moderate-toughness steels also show less stress-activated creep than do higher toughness steels, the extent of this cracking is much reduced as compared to that shown schematically in Figure B1 for very tough steels. Nevertheless, such materials can show measurable although modest time-dependent extension after pressure stops increasing, whose rate and extent depends on the time interval for the pressure hold, the relative stress level, and the extent to which toughness sustains cold creep. This growth is driven by stress-activated creep along the crack front and so reflects the same time-at-stress failure process[B7,B8] that is clearly apparent in the higher-toughness steels.

Higher toughness steels typically exhibit ductile fracture response across the range of practical service temperatures, whereas some pressure vessels and/or pipelines made of lower toughness steels operate below their ductile to brittle transition temperature (DBTT). Thus, as toughness

continues to decrease, it becomes necessary to consider toughness as well as the nature of the fracture response – because cracking can reflect a brittle mechanism such as cleavage versus a ductile process like microvoid nucleation, growth and coalescence. The least fracture resistant steels combine low toughness with brittle response. In contrast, some low toughness steels show 100-percent shear fracture at lower temperatures, but do not show macroscopic evidence of ductility in terms of lateral contraction or crack-tip blunting. Steels whose fracture is microscopically ductile that exhibit little dissipation aside from the energy to create new crack surface can be considered "fracture-brittle."

If the pressure stops increasing, measurable cracking ceases for fracture in brittle steels, while as noted above cracking can continue for moderate toughness steels. The response of fracture-brittle steels under plane-strain conditions is characterized by linear-elastic fracture mechanics[1] (LEFM) with the fracture resistance characterized by related test methods such as ASTM E399(B15). Cracking under increasing load in materials characterized by LEFM tends to be a go – no-go phenomenon. That is little or no time passes between the onset of cracking and its unstable rapid extension leading to immediate failure. LEFM admits limited nonlinear response due to plastic flow and little stable or arrested cracking, leading to load versus displacement response (analogous to pressure crack extension) such as that shown in Figure B2, which is reproduced from the above-noted test standard. It is apparent therein that for LEFM response, the difference between the maximum load and that associated with the onset of unstable cracking is very small, as plane-strain LEFM response effectively precludes stable crack extension without an increase in crack driving force. Figure B2 shows three idealized load-displacement plots that are used to qualify toughness determined according to this standard as an acceptable measure of LEFM fracture resistance. It is apparent from the load-displacement plots shown therein that little nonlinear response due to plastic flow. Figure B2 also shows that LEFM admits a small amount of stable or arrested cracking, which is apparent in Figure B2 through the notation "pop-in" and related limitations on the extent of stable cracking. Finally, for LEFM response, the difference between the maximum load and that associated with the onset of unstable cracking is small, as LEFM response effectively occurs without stable crack extension unless the crack driving force increases. Thus, the termination of the trends in Figure B2 effectively corresponds to the end of the blunting trend in Figure B1.

[1] Reference B2 and other such textbooks discuss this topic at length.

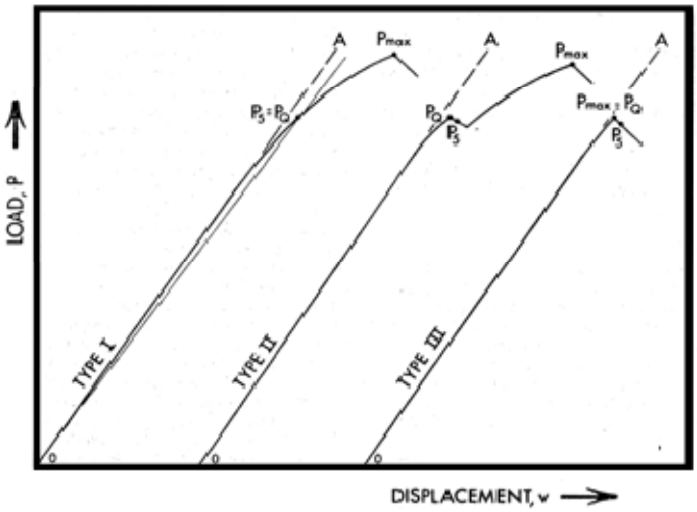

Figure B2. Schematics of idealized load-displacement response used in ASTM E399

In reference to Figure B1, the failure pressure for sharp axial defects under plane-strain conditions in fracture-brittle line pipe occurs at the intersection of the vertical line, and the first trend encountered labeled "initiation." Whether leak or rupture occurs as such cracks transition through-wall depends on the same factors noted earlier.

Under plane-stress conditions, fracture-brittle materials can experience limited stable extension and show some increase in bulging prior to failure. Continued extension in such line pipe steels occurs with increasing pressure. Such materials tend not to show measurable crack extension after pressure stops increasing. The stable extension and failure response in such cases is well characterized by LEFM and associated test methods like ASTM E561-98[(B16)]. Less growth and reduced time dependent cracking is anticipated for these steels as they show reduced stress-activated creep as compared to higher toughness steels, as will become evident shortly. Full-scale test data[(e.g., B17,B18]] indicate the extent and stability of such cracking is very sensitive to minor changes in pressure (local stress level).

Failure in reference to Figure B1 for plane-stress situations in fracture-brittle line pipe occurs along the curved pressure versus depth segment labeled therein "stable." Less tough steels or scenarios closer to plane-strain occur at lower pressures along this segment, and so involve relatively small amounts of crack extension prior to failure. Such stable crack extension is termed "subcritical," the notion being that cracking leading to immediate failure is "critical". In contrast to the response of less-tough steels, as toughness increases or conditions more favorable to plane stress develop, failure occurs at higher pressures along this segment, at correspondingly larger crack extension. Whether the breach created when this extension transitions through-wall causes a leak or a rupture depends on the same factors noted above.

Summary

It is evident from Figures B1 through B3 that significant differences can be experienced if the circumstances involved with the periodic hydro-retesting of Bobtail tanks promoted a breach of the tank wall. However, because Appendix A makes clear failure during a hydrotest is not likely

because any cracking of a size that could breach the wall is visually apparent, even without a rust stain, it is unlikely these differences would ever be practically significant or manifest in such testing. Appendix A also makes clear such cracking, were it to breach the wall would do so as a leak, which with water as a test medium would not pose significant safety issues.

Technology Aspects

Appendix A made use of results generated via plastic collapse and fracture mechanics which are briefly outlined next.

THE FRACTURE AND PLASTIC COLLAPSE MODELS

Fracture-controlled growth was quantified by the ductile flaw-growth model (DFGM), which has its roots in J-Tearing theory which in turn is based on the nonlinear fracture mechanics (NLFM) general crack driving force known as J-Integral. Like other fracture-based formulations, the DFGM compares a measure of crack driving force quantified in terms of J-integral to a measure of the materials resistance to cracking quantified in terms of J-integral known as the J-Resistance (J-R) curve. In applications to assess structural response where failure is possible by plastic collapse as well as fracture, the DFGM is coupled with a plastic-collapse analysis (PCA). The formulation and format of this PCA is like that of Battelle's recently developed collapse-based corrosion criterion for fully ductile behavior known as PCORRC, and its more general numerical form known as PCORR, which are detailed elsewhere[(e.g., B19-B22)]. This PCA compares a measure of local (net-section) stress to the materials capacity which in the simplest of cases is represented by the ultimate tensile stress (UTS). The essential difference between the PCA coupled with the DFGM and PCORRC is that the PCA was calibrated using numerical results from finite element analysis (FEA) for notches and groove-like defects, while PCORRC reflects numerical results for blunt defects typical of corrosion.

Because much has been done in the NLFM community over the almost 20 years since the original formulation of the DFGM was released, modest improvements have been made to the numerical calibration of this model by refining the underlying tables. This affects smoothing of its predictions as opposed to causing inherent differences in its capability or outcomes. In the same way much has been done at Battelle to enhance the PCA, for which much work was possible. Examples in this context include improved correlations of material response, such as for strain-hardening exponent and yield to tensile (Y/T) ratio[(e.g., B11)] and criteria to better relate multiaxial states of stress and strain to that under uniaxial tension[(e.g., B4)]. Consider now concepts that underlie the DFGM.

In the theory of elastic-plastic fracture mechanics, the J-integral is a valid crack driving force parameter that characterizes the intensity of the Hutchinson-Rice-Rosengren (HRR) fields for plastic and primary creep deformation which occurs after the initial elastic-plastic loading, and increases with time. As with any such fracture theory, when J reaches the critical toughness level, denoted J_{1C}, for plane strain and J_c for plane stress. Below this critical level defects whose severity is characterized by J are stable and without any evidence of tearing (void nucleation, growth, and coalescence to produce crack surfaces). Above this critical level, cracking via this same mechanism develops, which can be stable or at initiation immediately unstable. Because

the onset for tearing is determined in a general framework that accommodates elastic response, crack initiation in this formulation is coincident with its occurrence predicted within linear-elastic fracture mechanics (LEFM). As such, the DFGM can be applied to response in both regimes, provided the material response is correctly captured in the J-R curve. Beyond initiation crack growth continues with increasing J, consistent with the material's resistance to stable tearing characterized by the J-integral in the J-R curve. In all ways J-Tearing theory and concepts parallel those of LEFM except that with this driving force their application is valid for less confined inelastic action.

According to J-Tearing theory, cracking occurs wherever the above noted metrics for crack advance are satisfied. It follows that in addition to load-controlled situations identified by Garwood as candidates for cold creep, stable tearing via this mechanism is plausible under global or local displacement control, with extension continuing so long as those metrics are satisfied.

Tearing Resistance and Stress-Strain Response

The *J*-R curve is an experimentally determined measure of material resistance to tearing, from a stable state into initiation and beyond through stable crack extension and then instability. The viability of any *J*-based formulation is directly dependent on the viability of the *J*-R curve and its ability to correctly portray cracking response in the structural application. That is the analytical measure of crack driving force must be defined and determined consistent with the measure of the material's resistance to that driving force, and appropriately reflect the degree of constraint as well as any directional aspects of the material's response.

Experiments indicated that *J*-R curves are very similar for a particular class of steel that has been subject to similar processing. However, constraint induced by differences in local state of stress due for example crack depth or plate thickness, or the loading, can significantly alter initiation resistance. Such differences in constraint can be dealt with via a two-parameter *J*-based assessment[e.g., B3]. If toughness is determined following ASTM standard E1820 using the single-edge-notch bend (SENB) and compact-tension (CT) specimens that satisfy plane-strain requirements, then quite high crack-tip constraint develops and the *J*-R curve at initiation tends to a lower level. However, other specimens and practical components involve quite low constraint which means greater initiation resistance. In cases where crack-tip constraint is limited, as occurs for plane stress conditions, as demonstrated theoretically by Yuan and Yang[B23], numerically by Yan and Mai[B24] and experimentally by Schewalbe[B25], then a low-constraint specimen is viable, and there is no need to satisfy the usual plane-strain thickness requirements. Constraint can be considered low for axial extension of TW cracks, whereas depending on the length to depth of an axial PTW crack relative to the wall thickness the constraint can vary from low to high. It is essential in such cases to address these differences where very accurate solutions are essential.

Provided local strain rates are not particularly different, various loading conditions involving differences in load-hold time, or displacement rate, exert only a nominal effect on both crack initiation and extension. In contrast, strong temperature dependence is observed where thermally activated mechanisms contribute to cracking, for which *J*-R curves show a reduced resistance to tearing as temperature increases. As adapted in the DFGM, the *J*-R curve does not embed

significant constraint, as it is not typically essential for many pipeline applications, nor does it reflect thermally activated mechanisms. Accordingly, use of this formulation should be limited to lower homologous temperatures, say less than 300ºF for typical pressure vessel and line-pipe steels. Most applications of the DFGM have been made using *J*-R curves developed via using standard CT specimens and loading conditions in full-wall thickness specimens. Correlations between the parameters that characterize the J-R curve and more usual pipeline metrics of toughness like the CVN energy facilitate use of the DFGM, but care must be taken to ensure these reasonably reflect flaw initiation and growth for the application in hand.

The stress-strain curve was represented in a Ramberg-Osgood (R-O) relationship in formulating the DFGM. This form generalizes this relationship to incorporate time dependent behavior. Stress-strain data needed to quantify yield, hardening rate, and time dependence to calibrate this equation for applications to a given steel. Usual full-range displacement-controlled tensile tests define the yield and hardening R-O parameters.

The DFGM was formulated in analogy to the usual time-independent J-estimation scheme developed by Kumar and Shih[B26] for EPRI, with the necessary functions quantified via numerical analysis for through-wall (TW) cracks and part-through wall (PTW) cracks in thin-walled end-capped cylinder viable for vessel and pipeline applications[e.g., B27-B29].

Finite Element Validation of *J*(t) theory and the *J*-Estimation Scheme

Finite-element analysis (FEA) was done in regard to SENB and center-cracked panel (CCP) geometries made of specific grades of steel in the context of the full-wall thickness for line pipe applications. This FEA duplicated the loading history considered for the cases considered, with the FEA results showing that the simple estimation scheme reasonably characterized the time-dependent J-integral during primary creep straining[e.g., B30]. Accordingly, detailed numerical analysis was not found necessary as the simple analog noted above proved viable.

Experimental Validation of *J*-Estimation for SENB Specimens

For the SENB specimens with different crack sizes in X52 pipeline steel, it was observed that in all cases all of the crack growth occurred during the load-holding period, where the crack growth was creep dominated. The results indicate that the estimation model gave good predictions of the primary crack growth behavior that the experimental specimens experienced[e.g., B31]. In contrast, predictions that neglect time-dependent crack growth behavior may lead to non-conservative results for both failure load and failure time.

Adaptation and Validation for Axial PTW Cracked Cylinders

This analysis and the algorithm tracked are analogous to that outlined above for the laboratory geometries, but here the geometry involved axial cracks in a cylinder, with provision for bulging. As these aspects are detailed in the published literature[B27-B31], this detail is not replicated here. The validity of the DFGM and the related PCA has been evaluated by comparison of its predictions with the failure pressure and cracking response for a wide range of full-scale burst-pressure tests using 1) patched through-wall axial defects to evaluate instability predictions and 2) surface-defected pipe sections results to evaluate initiation and growth predictions. This has included “blind” predictions made as part of a “round-robin” evaluating the various failure

criteria for pipelines[B37]. In total predictions have been made for more than 100 experiments and field failures involving commercial grades whose yield stress ranged from 42 ksi up to 80 ksi, in toughness levels that run from a few ft-lbs up to levels beyond 150 ft-lb.[B7,B17,B32-B37]

Summary

Predictions made with the fracture and collapse models noted above did not show any particular bias as a function of observed burst pressure, nor is there bias in predicted failure behavior in regard to pipe size, defect size, steel grade or processing history, or toughness. Much of this was assessed in a statistical analysis that showed the mean value of predicted to actual failure pressure = 0.979, a standard deviation of 0.131, and an R^2 statistic of 0.93. It follows that the technology adopted for the analyses reported in Section 6 of the main report is viable for practical applications.

REFERENCES

B1. Anon., ASTM Standard E1820-99, Measurement of Fracture Toughness, ASTM 03.01.

B2. for example see Broek, D., "Engineering Fracture Mechanics," Nordhoff, 1974; Rolfe, S. T. and Barsom, J. M., "Fracture and Fatigue Control in Structures," Prentice-Hall, 1977.

B3. Zhu, X.K. and Leis, B.N., "Application of Constraint-Corrected J-R Curve to Fracture Analysis of Pipelines," J Press Vessel Tech, Vol 128, 2006, pp. 581-589.

B4. Zhu, X.K. and Leis, B.N., "Average Shear Stress Yield Criterion and its Application to Plastic-Collapse Analysis of Pipelines, I. J, Press. Vessels and Piping, Vol 83, 2006, pp. 663-671, see also Zhu, X.K. and Leis, B.N., "Theoretical and Numerical Predictions of the Burst Strength of Pipelines," J Press. Vessel Tech, ASME, Volume 129, 2007, pp.

B5. Kiefner, J. F., Maxey, W. A., and Eiber, R. J., "A Study of the Causes of Failures of Defects That Have Survived a Prior Hydrostatic Test", NG-18 Report No 111, November 1980.

B6. Duffy, A. R., McClure, G. M., Maxey, W. A., and Atterbury, T. J., "Study of the Feasibility of Basing Natural Gas Pipeline Operating Pressure on Hydrostatic Test Pressure," Pipeline Research Council International, PRCI/AGA Catalog No. L30050, 1968.

B7. Leis, B. N., Brust, F. W., and Scott, P. M., "Development and Validation of a Ductile Flaw Growth Analysis for Gas Transmission Line Pipe," PRCI/AGA Catalog No. L51543, Pipeline Research Council International, June 1991.

B8. Riedel H and Rice J R, "Tensile cracks in creeping solids", Fracture Mechanics, ASTM STP 700, American Society for Testing and Materials, pp.112-130, 1983

B9. Leis, B. N., "Hydrostatic Testing Of Transmission Pipelines: When It Is Beneficial and Alternatives When It Is Not", PRCI Report PR-3-9523, Pipeline Research Council International, 2001.

B10. Leis, B. N., Walsh, W. J., and Brust, F. W., "Mechanical Behavior of Selected Line Pipe Steels", NG-18 Report No. 192, PRCI Cataolg No. L51624, 1990.

B11. Zhu, X.K. and Leis, B.N., "Influence of Yield-to-Tensile Strength Ratio on Failure Assessment of Corroded Pipelines," in Application of Fracture Mechanics in Failure Assessment, ASME, PVP-Vol.462: pp. 23-30, 2003.

B12. Leis, B. N. and Brust, F. W., "Ductile Fracture Properties of Selected Line-Pipe Steels", NG-18 Report No 183, PRCI Catalog Number L51604, 1990.

B13. Leis, B. N., "Ductile Fracture and Mechanical Behavior of Typical X42 and X80 Line-Pipe Steels", NG-18 Report No. 204, A. G. A. Catalog No. L51682, 1992.

B14. Leis, B. N. and Brust, F. W., "Hydrotest Strategies for Gas Transmission Pipelines Based on Ductile Flaw Growth Considerations," PRCI/AGA Catalog No. L51665, Pipeline Research Council International, 1992: see also Leis, B. N., "New Insights into Hydrostatic Testing and Retesting," Proceedings of the 1993 A.G.A. Operating Section, American Gas Association Catalog No. X59707, pp 532 543, 1993.

B15. Anon., ASTM Standard E399-99, Plane-Strain Fracture Toughness of Metallic Materials, ASTM 03.01

B16. Anon., ASTM Standard E561-98, R-Curve Measurement of Fracture Toughness, ASTM 03.01.

B17. Olson, R. J., Narendran, V. K., Leis, B. N., Kilinski, T. J., Scott, P. M., and Gertler, R. C., "Full-Scale Testing to Validate PAFFC and Develop Data to Assist Evaluating the Benefits of Hydrotesting", Appendix 7 of Leis, B. N., "Hydrostatic Testing of Transmission Pipelines: When It Is Beneficial and Alternatives When It Is Not," PRCI Catalog No. L51844, Pipeline Research Council International, 2001.

B18. Kiefner, J. F., Maxey, W. A., and Eiber, R. J., "A Study of the Causes of Failures of Defects That Have Survived a Prior Hydrostatic Test", NG-18 Report No 111, November 1980.

B19. Leis, B. N. and Stephens, D. R., "An Alternative Approach to Assess the Integrity of Corroded Line Pipe – Part Two: Alternative Criterion", 7th International Conference on Offshore Pipelines and Polar Engineering, Vol. 3, pp 635 – 641, 1997: see also Leis, B. N. and Stephens, D. R., "An Alternative Approach to Assess the Integrity of Corroded Line Pipe – Part One: Current Status", 7th International Conference on Offshore Pipelines and Polar Engineering, Vol. 3, pp 624 – 634, 1997.

B20. Stephens, D. R. Leis, B. N., and Rudland, D. L. "Development of a New, Simplified Criterion for Pipeline Corrosion Defect Limit States", 11th PRCI/EPRG Biennial Joint Technical Meeting on Line Pipe Research, pp 13.1-18, Arlington, 1997.

B21. Stephens, D.R. Leis, B.N., Kurre, M.D., and Rudland, D.L. "Development of an Alternative Failure Criterion for Residual Strength of Corrosion Defects in Moderate- to High-Toughness Pipe" Battelle Report to PRCInternational, PRCI L51794, 1999.

B22. Stephens, D.R. and Leis, B.N., "Development of an Alternative Failure Criterion for Residual Strength of Corrosion Defects in Moderate- to High-Toughness Pipe", International Pipeline Conference, Vol. 2, pp. 781-792, ASME, Calgary, 2000.

B23. Yuan, F.G. Yang, S., "Crack-tip Fields in Elastic-Plastic Material under Plane Stress Mode I Loading, Int J Fract, Vol. 85, 1997, pp. 131-155.

B24. Yan, C. and Mai, Y.W., "Numerical Investigation on Stable Crack Growth in Plane Stress," Int J Fract, Vol. 91, 1998, pp. 117-130.

B25. Schawalbe, K.H., "Ductile Crack Growth under Plane Stress Conditions: Size Effects and Structural Assessment – I. Size and Geometry Effects on Crack Growth Resistance," Eng Fract Mech, Vol. 42, 1992: pp 211-219.

B26. Kumar, V., German, M. D., and Shih, C. F., "An Engineering Approach for Elastic-Plastic Fracture Analysis," EPRI Report # NP-1931, Electric Power Research Institute, 1981.

B27. Stonesifer, R. B., Brust, F. W., and Leis, B. N., "Stress-Intensity Factors for Long Axial Outer Surface Cracks in Large R/t Pipes," ASTM STP 1131, American Society for Testing and Materials, Philadelphia, 1992, pp. 29-45.

B28. Brust, F. W., and Leis, B. N., "A New Model for Characterizing Primary Creep Damage," I J Fract, Vol. 54, pp 45-63, 1992.

B29. Brust, F. W., and Leis, B. N., "A New Model for Predicting Primary Creep Damage in Axially-Cracked Cylinders: Part I – Theory," Engr Fract Mech, Vol. , pp, 1992: see also Brust, F. W., and Leis, B. N., "A New Model for Predicting Primary Creep Damage in Axially-Cracked Cylinders: Part II – Application ", Engr Fract Mech, Vol. , pp, 1992

B30. Brust, F. W., and Leis, B. N., "A Study of Primary Creep Crack Growth at Room Temperature," Proceedings 5th International Conference on Numerical Methods in Fracture Mechanics, 1990, pp 321-332.

B31. Leis, B. N., and Brust, F. W., "Validation of Room-Temperature Primary Creep Crack Growth Analysis for Surface-Cracked Pipes", Nuclear Engineering and Design, Vol. 142, 1993, pp. 69-75.

B32. Kiefner, J. F., Maxey, W. A., Eiber, R. J., and Duffy, A. R., "Failure Stress Levels of Flaws in Pressurized Cylinders", Progress in Flaw Growth and Fracture Toughness Testing, ASTM STP 536, American Society for Testing and Materials, 1973, pp 461-481.

B33. Williams, D. N. and Maxey, W. A., "Evaluation of an X70 Low-Carbon Bainitic-Steel Pipe (EF), NG 18 Report 145, September, 1985

B34. Williams, D. N. and Maxey, W. A., "Evaluation of an X70 Pipe Fabricated from an Accelerated-Cooled C-Mn-V-Cb Steel (EN), NG 18 Report 157, May, 1986

B35. Williams, D. N. and Maxey, W. A., "Evaluation of an X70 Pipe Fabricated from an Accelerated-Cooled Boron Containing Steel (EO), NG 18 Report 161, August, 1986

B36. Williams, D. N. and Maxey, W. A., "Evaluation of an X80 Pipe Fabricated From Controlled-Rolled Steel (EM), NG 18 Report 169, November, 1987

B37. Anon., Report of the Public Inquiry Concerning Stress Corrosion Cracking on Canadian Oil and Gas Pipelines, National Energy Board (Canada), Proceeding MH-2-95, November 1996, pp. 135-139.

APPENDIX C:
PHOTOS OF VARIOUS PROPANE CARGO TANK CHASSIS AND MOUNTING METHODS

APPENDIX D:
ANALYSIS OF FACTORS CONTROLLING OR LIMITING GENERALIZING DEFECT RESPONSE AND LEAK BEFORE RUPTURE FOR BOBTAIL PROPANE TANKS REFERENCED TO SA-612

APPENDIX D:
ANALYSIS OF FACTORS CONTROLLING OR LIMITING GENERALIZING DEFECT RESPONSE AND LEAK BEFORE RUPTURE FOR BOBTAIL PROPANE TANKS REFERENCED TO SA-612

BACKGROUND

The body of this report considered analysis of the Trinity Signature bobtail unit, which is made of SA-612. A broad range of prior work [e.g., Leis 2001] has shown that the small differences in tank geometry as occur across the range of Bobtail tanks do not appreciably alter the outcomes presented in Figures 24 to 27. Accordingly, the outcomes developed specifically for the Trinity-Signature unit are relevant across the range of bobtail tank geometries in use.

The body of the report also makes clear that the analysis that gave rise to Figures 23 to 26, which was presented in Appendix B, involves the mechanical and fracture properties of the steel, both of which can significantly influence the outcomes presented in Figures 23 to 26. Most critical in this context was the UTS, which controls failure by plastic collapse, and the toughness quantified in terms of CVN energy, which controls failure by fracture as quantified in Figures 25 and 26. Elongation to failure was also noted to be important, because it reflects the ductility of the steel involved. Because toughness in general remains uncertain for most any bobtail tank regardless of the grade, the outcomes developed specifically for the Trinity-Signature unit (Figures 23 to 26) were presented as a function of toughness after which Grade SA-612 was reviewed relative to the toughness anticipated for such tanks made of SA-612 in the late 1980s and thereafter. Literature data coupled with information specific to usual production of SA-612 plate was used to infer its toughness being well in excess of 5 ft-lb, being typically at levels that preclude concern for fracture controlled failure under bobtail hydrotest conditions.

Subsequent consideration of other grades in the body of the report focused specifically on two grades – SA-202 and SA-455. That discussion noted that the circumstances of production coupled with the requirements of those specifications did not broadly support generalization of the conclusions reached in regard to SA-612 produced after the 1980s shift to the use of this grade, and made reference to this Appendix as the basis for that observation. Thus, the objective of this appendix is to establish conditions under which the outcomes for SA-612 [*] produced after the 1980s shift to the use of this grade can be extended to tanks made of grades SA-202 and/or SA-455.

Objective and Approach

[*] While the ANSI format for such specifications differs somewhat from the format adopted by the ASTM, the content of the ANSI "SA" specification and the ASTM specification is comparable. As such, this Appendix does not discriminate between the versions of specification, and simply adopts the ANSI designation to indicate which specification is being considered.

Clearly, the outcomes for tanks made of SA-612 produced after the 1980s shift to the use of this grade can be extended to tanks made of grades SA-202 and/or SA-455 if it can be shown that the corresponding properties for the tank in question are equal or exceed that for SA-612. As such, case-specific data for a given tank can be used to satisfy this requirement by direct evaluation use of such data in Figures 25 and 26.

As case-specific tank data have not historically been developed, the objective of this appendix must be considered in a more general setting, which involves assessing if the specifications for grades SA-202 and/or SA-455 can consistently be shown to ensure the properties equal or exceed that for SA-612. Accordingly, this appendix compares and contrasts the specifications for each of the grades SA-202 and SA-455 to SA-612.

Grade SA-612 in Contrast to Historic Grades

Ideally, the compare-contrast process would make use of the specifications in force in the era that the tank was manufactured, as such specifications can change over time – and typically become more stringent. But, as it is expedient to assess the current specifications and thereafter assess in retrospect the implications of changes over time, as necessary, this approach has been adopted.

Recognizing that SMYS for the three grades involved differs, which in turn affects thickness, the assessment considers the subgrade closest to that applicable to the SA-612 scenario. Thus, for SA-202, subgrade B (SMYS = 47 ksi) is used for this assessment, as it is closest to 50 ksi, which applies for the SA-612. For SA-455, the subgrade for the mid-range thickness (0.375 to 0.580 inch) associated with SMYS = 37 ksi yield is used for this assessment, as this thickness interval is closest to that for the Trinity-Signature unit, and also broadly relevant to bobtail tanks. Because the values of SMYS differ across these grades, the outcome of what follows is not a direct comparison with Trinity-Signature unit.

The specifications for the three grades of concern incorporate specification A20 / A20M (ASTM 2010) by reference, along with several other specifications. Specification A20 / A20M covers provisions common to all three grades, which means it in no way discriminates between these grades, and so is not considered further. As this is the case for all specifications that are incorporated by reference, they too are considered no further. Only the UTS, the CVN energy, and the Elongation are considered as these are the metrics that influence the outcomes in Figures 24 to 27, along with factors that indirectly control these parameters that are otherwise embodied in these three specifications, the results of which are summarized in Table D1.

Table D1. Key aspects of Grades SA-612, SA-202, and SA-455

Parameter	Specification[d]		
	SA-612	SA-202 GrB	SA-455[c]
SMYS[a], ksi	50	47	37
UTS, ksi	81 – 105[b]	85 to 110	73 to 95
% Elongation (in 2 inch gage)	22	18	22
C /Mn / P / S, maximum heat wt%	0.25 / 1.50 / 0.035 / 0.025	0.25 / 1.40 / 0.035 / 0.040	0.33 /1.20 / 0.035 / 0.035

a) For the subgrade selected (see text above).
b) This interval brackets all subgrades.
c) For thickness bounded below by 0.375 inch and above by 0.580 inch.
d) ASTM and ASME SA specifications are "identical" with last current ASTM values reported.

UTS as a Metric

Consider first the UTS. As Table D1 indicates, for SA-612 and tank thicknesses 0.5-inch and above, the UTS ranges from 81 to 101 ksi, while thinner sections it ranges from 83 to 106 ksi, an interval involves a swing of 28%. This is a significant range for the UTS, which as noted above controls the failure response for plastic collapse. This broad interval implies a broad range of chemistries and processing can satisfy this aspect of SA-612, which is consistent with the scope of shared chemistries noted in A20 / A20M and the limits specified for this grade. Because the UTS controls the failure pressure for failure via plastic collapse, a lower-bound value of the UTS must be adopted, which for the analyses that underlie Figures 24 and 25 was 81 ksi. For SA-202 the range for the UTS is 85 to 110 ksi (a swing of 29%) for SMYS at 47 ksi (i.e., Gr B), whereas for SA-455 the range for the UTS is 73 to 95 ksi or 30% (the largest swing in UTS).

As for SA-612, the broad interval for values of UTS for both SA-202 and SA-455 implies a broad range of chemistries and processing can satisfy this aspect of those specifications, which is anticipated given the scope of shared chemistries as noted in A20 / A20M and the specific limits for these grades. Again, because the UTS controls the failure pressure for failure via plastic collapse, a lower-bound value of the UTS must be adopted, which for SA-202 is 85 ksi while that for the SA-455 is 73 ksi. It follows that failure of the these historic grades relative to the current grade occurs at pressures relative to that for SA-612 at about a ratio of 85/81 or 105% for SA-202 and 73/81 or 90% for SA-455. Thus, in regard to the UTS as a metric, the outcomes of Figures 26 and 27 are transferrable for the SA-202, but not for the SA-455.

Elongation to Failure as a Metric

Consider next the Elongation to failure. As Table D1 indicates, for SA-612 the minimum Elongation to failure is 22% (in a 2-inch gage), and is independent of thickness, which is also the case for SA-455, whereas this minimum is 18% for the SA-202. As this metric is an indicator of ductility, which can in turn point to improved toughness, one can infer that relative to Elongation the outcomes of Figures 25 and 26 are transferrable for the SA-455, but not for the SA-202.

Toughness as a Metric

Finally, consider results relevant to toughness, which given its central role in Figures 23 to 26 is perhaps the most critical of the three metrics noted. Both SA-612 and SA-202 include

comparable special requirements provisions, which provide for CVN testing as mutually agreed, but do not require it. It follows that for these grades there is a better chance for CVN data to be available than for SA-455, which has much less general special provisions that do not provide for CVN testing – suggesting that that toughness is not a concern for those building tanks during the time interval that grade was popular.

While CVN values are of greatest utility in regard to Figures 23 to 26, as its measurement is not directly specified for any of the grades of interest, a surrogate must be identified for purposes of this compare and contrast process. The literature was evaluated with a view to identify a surrogate for CVN energy based on the steel chemistry relative to the specified chemistry for each of the grades. This should be a viable approach in that the literature indicates steel chemistry and more specifically cleanliness and sulfide shape control are important factors in regard to toughness [e.g., Gray 2009]. A check of the three specifications indicates that SA-612 and SA-202 specify the same broad range of elements covering Carbon (C), Manganese (Mn), Phosphorus (P), Sulfur (S), Silicon (Si), Copper (Cu), Nickel (Ni), Chromium (Cr), Molybdenum (Mo), and Vanadium (V), while SA-455 covers just the first five – that is C, Mn, P, S, and Si. Of these, possible surrogates for CVN include C, Mn, P, and S. These are the most likely surrogates because high carbon can be associated with brittle response, Mn needs to be present to combine to form the MnS inclusions known to lead to lower toughness, and high levels of both P and S can be metrics of "dirty" steel.
Because Battelle has a long history involved with steels in use as pressure boundaries, either for vessels or for line pipe and process piping, file data were gathered to support trending as a function of CVN energy. In excess of 300 data sets were located covering grades bounded by $42 \leq \text{SMYS (ksi)} \leq 80$, with only matched datasets used involving FSE CVN along with C, Mn, P, and S used for this assessment. The data were organized and trended relative to toughness, with C showing high correlation, which also occurred for P and S, whereas Mn was not well correlated. Figure D1 serves to illustrate the trended data developed, which is specific to sulfur.

The trend in Figure D1 shows that as sulfur content diminishes the toughness increases, but also shows a quite broad scatter-band. Such was also the case for C and P. While sulfur (as well as C and P) did correlate with toughness, the scatter indicates that there are other factors involving the chemistry and processing and the CVN testing that affect correlation quality. Toward the top of Figure D1 there is a timeline relative to the x-axis that indicates typical sulfur levels in steel produced in 1975, 1980, and 1995 (e.g., [Gray 2009]). Also shown in this figure are the specified levels for sulfur for three grades of interest.

It is apparent from the three specified maximum levels that the level for SA-612 is about three-quarters of that for SA-202 and SA-455, which list higher maximum bounds. While the trend evident shows only a small reduction in the lower bound for the SA-202 and SA-455 as compared to SA-612, this small shift carries down into a regime of toughness that lies below the lowest value shown in Figures 25 and 26. On this basis, tanks made from the historic grades do not satisfy the same conditions that underlie the conclusions made in regard to SA-612 in the body of the report.

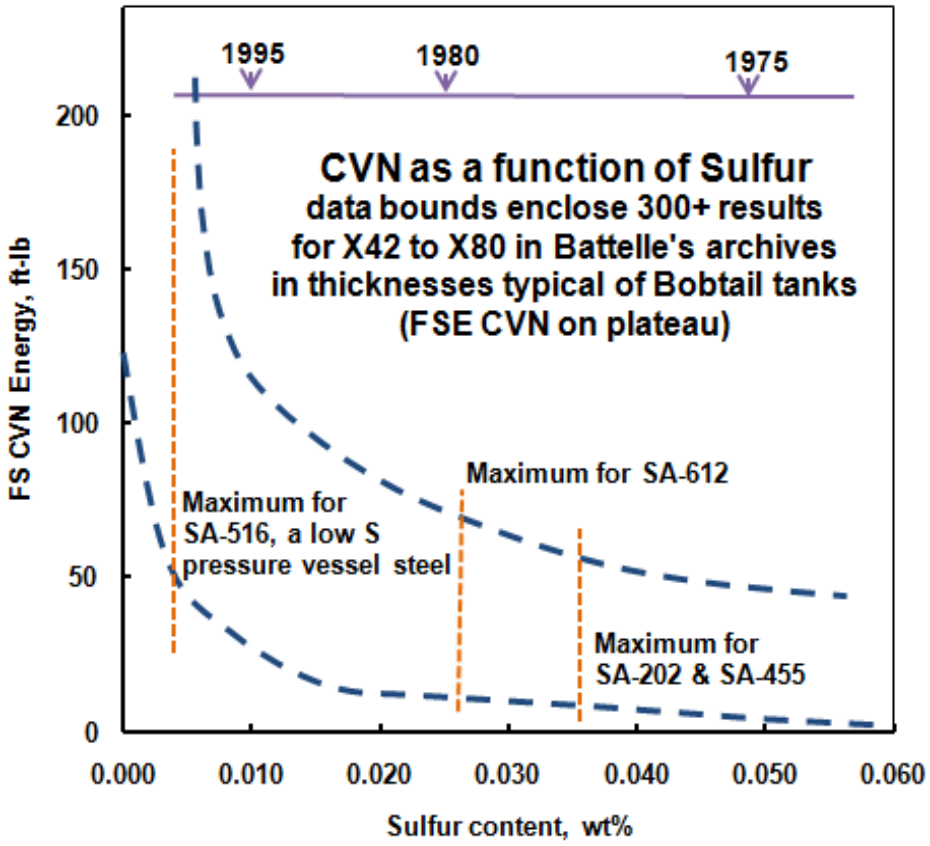

Figure D 1. Correlation between CVN energy and Sulfur level (Battelle archival database)

The timeline in Figure D1 was developed in reference to ArcelorMittal literature and similar published information (e.g., [Gray 2009]). It is evident from such information that the effects of melting practices and chemistry limits on sulfur have been understood and selectively in use to produce steel with high toughness since the 1970s – which over time has found broader utility and becomes typical of leading producers beginning in the early to mid 1980s. In this context, some steels such as SA-516 have been routinely available from some mills at sulfur levels as low as 0.001% since the mid to late 1970s.

As the bounds in Figure D1 reflect maximum levels, it is apparent that order of magnitude improvements in toughness can be anticipated in bobtail tanks made of SA-612 at levels modestly below its specified maximum. In contrast, a significant reduction below their specified maximum is required to affect a major improvement in toughness for tanks made of historic production involving other common grades. This observation coupled with the transition to SA-612 in the mid-1980s indicates the outcomes shown in Figures 23 to 26 is specific to that grade, which underlies the limitations on the use of those outcomes stated in the body of the report relative to SA-202 and SA-455 (and equally any other such historically used grades). Because C, P, and S were found to correlate with CVN, any one of these elements could be used as a surrogate for CVN energy for purposes of this assessment. Comparing the heat-based specifications in regard to C, P, and S, the outcomes in this sequence as maximum levels in

weight-percent were as noted in Table D1 for SA-612 as 0.25, 0.035, and 0.025, for SA-202 as 0.25, 0.035, and 0.040, and for SA-455 as 0.33, 0.035, and 0.035. The quality of the correlations developed in reference to Battelle's archival database is too uncertain to distinguish between these grades on carbon level, but was more sensitive in regard to P and S. But as Figure D1 introduced above illustrates, the scatter was significant. While as noted above either of C, S, and P could serve as a surrogate, it is evident from the comparison of these chemistries that only the limit on sulfur discriminates between these grades. Recognizing that the lower-bound trend in Figure D1 swings near 5 ft-lb for SA-455 and/or SA-202, in light of the trends with toughness in Figures 26 and 27 one must conclude that the statements made in regard to SA-612 in the body of the report are not transferrable to other historic grades in regard to toughness. This observation coupled with the conclusion of the prior text indicates that none of the metrics evaluated support general expansion of the outcomes in Figures 25 and 26 to applications that involve SA-455 or SA-202.

To this juncture, only the timeline in Figure D1 and vague reference to the literature support the assertion that the outcomes in Figures 25 and 26 are generally applicable to SA-612 production. Further insight into the timeline for sulfur control serves to validate this general applicability, with the quantitative timeline and trends shown in Figure D2 (after [Gray 2009]) providing a concrete basis for this view. Inspection of Figure D2 shows that it quantifies the presence of impurity elements as a function of time, wherein the impurity level is shown on a logarithmic scale in ppm on the y-axis as a function of the timeline shown on the x-axis. Figure D2 also shows the specific technology in typical use that was implemented to achieve the outcomes presented. The x-axis runs in time from 1970 through 1986, and while it ends in 1986, in many ways the trends beyond this point have changed very little since. This is because the necessary controls and practices were broadly in place to affect the benefits sought through impurity management by the early 1980s. In this regard, the levels shown circa 1986 continue forward over time, with little change going forward relative to that occurring over the prior decades. Figure D2 includes a range of what were termed impurities, which given carbon is included might be viewed as inappropriate labeling of the y-axis. For present purposes the solid trend labeled [S] for sulfur is relevant, as are those labeled [C] for carbon, and [P] for phosphorous.

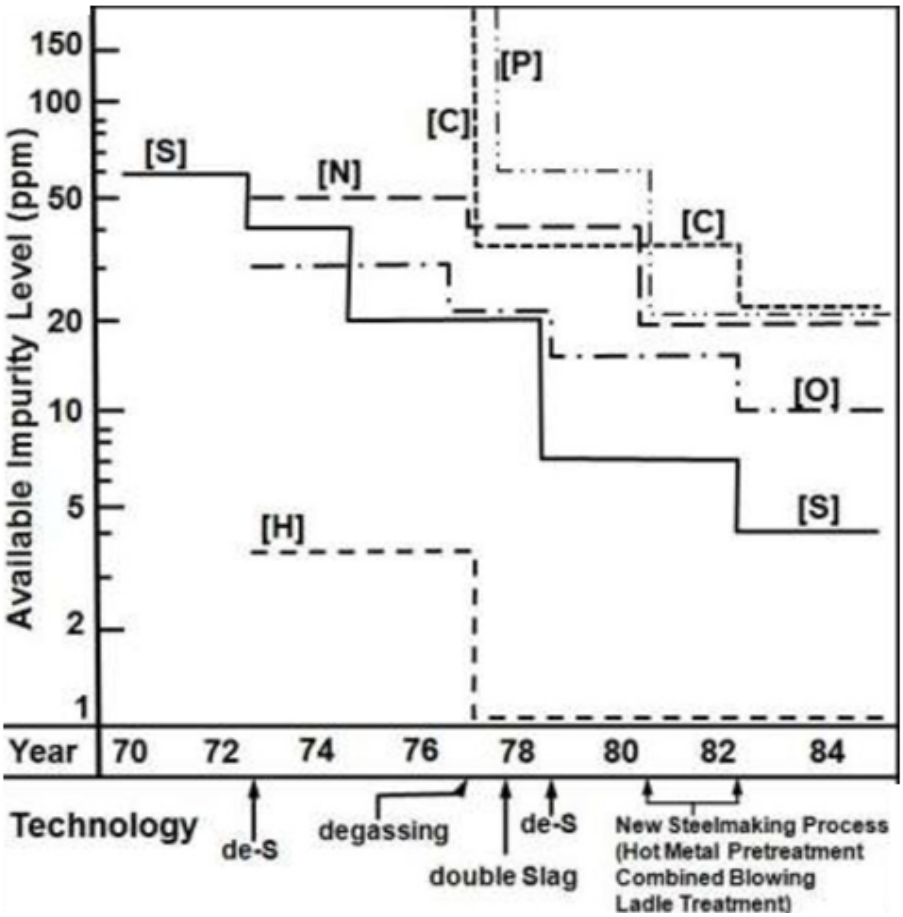

Figure D2. Timeline for sulfur levels mid-1980s vs historic production [Gray 2009]

Note in this context the level of sulfur in usual production has been reduced to 5 ppm by 1982, which from Figure D1 can be taken to infer toughness levels for the grade adopted for tank production about that time are generally acceptable in regard to the analyses outcomes shown in Figures 23 to 26. Thus, while those outcomes are specific to SA-612, in regard to Figure D2 these outcomes might be viewed as representative of steels produced with the technologies that Figure D2 identifies as "hot-metal" pretreatment. Hot-metal pretreatment as the figure implies involved processing of the melt prior to its being continuously cast (so-called concast steel) into strand, as feed to production of slabs from which cut slabs and plate is obtained. This specific type of processing was not done for steels produced using traditional ingot-based practices, such that this mill practice could serve as a preliminary means to sort tanks made via historic versus more modern steels.

The final point that must be addressed is the retrospective evaluation of how the above-noted observations could change due to time-related differences in the specifications of interest – which is done with the realization that specifications typically become more stringent as time passes. Because as evident earlier the maximum allowable level of sulfur was the primary discriminator between the specifications compared, this comparison focuses on this parameter. Figure D2 is key to this assessment, as it indicates patterns in sulfur levels over time, which as noted earlier change little in relative terms beyond 1986, with the minimum bound in that era

being first established in 1982 according to this figure. In this context, while some steels marketed as low sulfur have pushed below that level, the current maximum sulfur level specific to SA-612 is 0.025. This level is many times the minimum noted in Figure D2 such that there is nominally no reason to anticipate its decreasing over time. In contrast, the maximum sulfur level for the historic grades is already larger than for SA-612, and unlikely to have decreased in the interim. As such, there is no compelling basis to further explore the implications of changes over time, as there is no reason to anticipate it will alter the result based on comparing the current requirements.

In many ways the above observations are apparent in ASME VIII Division 2 Part3 guidance on toughness testing requirements for steels used in pressure vessels. While this guidance is applicable to more demanding pressure scenarios than the Bobtail tank, it is clear from the Toughness Testing Exemption Curves in this guidance that normalized SA-612 qualifies among the few grades identified therein as the toughest steels. In contrast, steels like SA-202 and SA-455 would be grouped in the worst category. In regard to that guidance, considering -40F as the lower-bound temperature of concern for a bobtail tank (for which the vapor pressure is near zero gauge), SA-612 satisfied that guidance for pressure vessel applications without the need for toughness testing, whereas steels like SA-202 and SA-455 require toughness testing to prove fitness for service.

Accordingly, while chemistry and related historic trends do not indicate that steels like SA-202 and SA-455 share the same traits as SA-612 produced since it has become the dominant steel used in producing bobtail tanks, this observation does not preclude their use provided adequate toughness can be demonstrated. Guidance in regard to a minimum toughness follows from analysis of fracture susceptibility, which as presented in the body of the report indicates a minimum of 10 ft-lb FSE CVN is appropriate – with other related details presented there.

CONCLUSIONS

It is apparent that steel production about the time the transition was made to SA-612 from the earlier used grades led to consistent production that supports the applicability of the outcomes shown in Figures 23 to 26 across that grade. In contrast, the results do not support the general extension of these outcomes to earlier production absent case-specific support in the form measured CVN values, or supplemental provisions to the purchase specification that make clear the tank steel will reliably resist crack growth consistent with that for the more modern production. While chemistry and related historic trends do not indicate that steels like SA-202 and SA-455 share the same traits as SA-612 produced since it has become the dominant steel used in producing Bobtail tanks, this observation does not preclude their use provided adequate toughness can be demonstrated. Guidance in regard to a minimum toughness follows from analysis of fracture susceptibility, which as presented in the body of the report indicates a minimum of 10 ft-lb FSE CVN is appropriate – with other related details presented there.

REFERENCES

ASTM 2010. ASTM Standard A20/A20M, 2010, "Specification for General Requirements for Steel Plates for Pressure Vessels," ASTM International, West Conshohocken, PA, 2003, DOI: 10.1520/A0020_A0020M-10, www.astm.org.